People's Democratic Republic of Algeria

Ministry of Higher Education and Scientific Research

UNIVERSITY OF KASDI MERBAH OUARGLA

Faculty of Mathematics and Material Sciences

Department of physics

THESIS

For obtaining the LMD Master Degree in physics

Specialty: Physics of Material

Presented by:

Hacini Nourehane

Entitled

Synthesis and characterization of nanocomposite thin film

Publicly defended on: 11/05/ 2025

supervisor	**Pr.Belakroum karima**	**Université de Ouargla**
Co-supervisor	**Dr.Besra Safa**	**Université de Ouargla**
examiner	**Pr Benmabrouk Lazher**	**Université de Ouargla**
President	**Maatouch Mouna**	**Université de Ouargla**


بسم الله الرحمن الرحيم

DEDICATION

I dedicate this work to:

My beloved parents, for their unwavering love and support,

My brothers and my sister, for their encouragement and motivation,

My dear nieces,

My entire family, for their love and backing,

And to all my friends, for their friendship and support.

ACKNOWLEDGEMENTS

"Firstly, we would like to extend our deepest gratitude to Almighty God, who has granted us the strength and courage to successfully complete this humble work. We would like to express our sincere appreciation to our supervisor, Dr. Belakroum Karima, and co-supervisor, Dr. Besra Safa, both lecturers at the University of Ouargla, for the opportunity they provided us by proposing this research topic and for their judicious guidance throughout the project. We are deeply grateful for the invaluable experience and expertise they shared with us through their precious advice and counsel.

We would also like to extend our gratitude to Professor Omar BENTOUILA for presiding over our thesis jury and to Dr. Sebti KHODJA for graciously accepting to be an examiner of this jury.

Our sincere thanks go to Professor Benmabrouk Lazher, Professor of Physics at the University of Ouargla, who warmly welcomed us to the Laboratory of Radiation, Plasma, and Surface Physics (LRPPS) at the University of Ouargla.

We would like to express our heartfelt appreciation to our teachers for the knowledge and wisdom they imparted to us and for the pleasant moments we shared with them during our five years of study. Special recognition goes to all our colleagues for their unwavering encouragement.

Finally, we would like to extend our special thoughts to our families, friends, and all those who supported us throughout our studies and particularly during the realization of this thesis.

Table of contents

List of figures

List of table

general Introduction

In recent years, a revolution has occurred in the field of materials physics, with a focus on the unique properties of materials at the nanoscale. Semiconducting metal oxides, such as ZnO and TiO2, have garnered significant attention due to their potential applications in various fields, including electromagnetism, optics, solar cells, and environmental remediation

Photocatalysis using solar radiation as a light source has emerged as a promising approach for environmental remediation. This technique has the potential to degrade organic pollutants, rendering them non-toxic or less toxic. The use of semiconducting metal oxides, such as ZnO and TiO2, as photocatalysts has shown great promise in this field

Various physicochemical and biological techniques, such as chemical oxidation, filtration, and adsorption, are currently employed for pollution treatment. However, these techniques may be ineffective or costly. Photocatalysis using solar radiation offers a viable alternative for the degradation of organic pollutants.

In recent years, significant advancements have been made in the deposition techniques of thin films, enabling precise control over film thickness and uniformity. Various techniques, including electrodeposition, pulsed laser deposition, sputtering, sol-gel, and spray pyrolysis, have been employed to deposit thin films. Among these, the sol-gel method is a popular and promising technique due to its economic feasibility and ease of use.

This study aims to synthesize and characterize ZnO-CuO-composite thin films with varying CuO concentrations (10%, 20%, and 30%) using the sol-gel spin coating technique on glass substrates. The structural, optical, and morphological properties of these films will be investigated, along with their photocatalytic activity.
This research will be organized into three main chapters. Chapter I will provide a general overview of transparent conducting oxides, with a focus on zinc oxide and copper oxide, and their unique properties.

Chapter I: Transparent Conducting Oxides This chapter will review the theoretical background of transparent conducting oxides, including their definition, properties, and classifications. The focus will be on zinc oxide and copper oxide, with a discussion of their unique properties and potential applications.

Chapter II: Deposition Methods This chapter will review the main deposition methods used to prepare thin films, including the sol-gel method. The advantages and disadvantages of each method will be discussed, with a focus on the sol-gel method, which will be used in this study. Chapter III: Preparation and Characterization of Thin Films This chapter will cover the preparation of thin films of zinc oxide and copper oxide using the sol-gel method. The properties of these films, including their structural, optical,

and morphological properties, will be investigated. The results will be analyzed and discussed, with a focus on the effects of doping ratio and film thickness on the final properties of the thin films.

Chapter1 : Bibliographical review on zinc and copper oxide and its applications

I-Introduction:

The study of transparent conductive oxides (TCOs) began in the early 19th century. These materials are considered essential in the fabrication of optoelectronic devices, particularly in the production of thin-film technologies. Over time, several studies and discoveries have emerged concerning TCOs. Key milestones include the following:

- In 1954, the first use of a transparent conductive oxide was reported following the discovery of tin-doped indium oxide (In_2O_3:Sn), known as ITO, by the scientist G. Rupprecht.
- By 1960, other binary oxide compounds such as zinc oxide (ZnO), tin oxide (SnO_2), and indium oxide (In_2O_3) were identified as transparent conductive materials.
- In 1980, ternary oxide compounds such as cadmium indium oxide ($CdIn_2O_4$) and cadmium tin oxide (Cd_2SnO_4) also emerged as notable TCOs.

It was observed that most of these TCOs exhibit n-type conductivity, whereas achieving p-type conductivity remained challenging. However, in 1993, H. Sato and colleagues succeeded in developing p-type transparent conductive oxides, particularly copper aluminum oxide ($CuAlO_2$), with enhanced electrical performance, although their conductivity was still lower compared to n-type materials. This achievement marked a significant milestone in the development of both n-type and p-type TCOs. This study aims to explore the concept of transparent conductive oxides, highlight their applications, and explain the crystal structure of these oxides, which will be further detailed in the following chapters[12,1].

I.1 Transparent Conducting Oxides:

I-1-1Definition :

Transparent Conducting Oxides (TCOs) represent a unique class of materials that concurrently exhibit high electrical conductivity and optical transparency[12,2].The origin of their conductivity lies in the presence of excess electrons, which arise from structural defects, stoichiometric deviations in the oxide lattice, or deliberate doping with appropriate dopants[12,3].

I-1-2 Types of transparent conducting oxides:

Transparent Conducting Oxides (TCOs) are commonly binary metal oxides that exhibit degenerate semiconductor behavior[2]. The Fermi level in these materials is positioned near or within the conduction band, particularly at high doping levels. This results in a high concentration of electrons in the conduction band at room temperature, enabling electrical conductivity. Furthermore, TCOs possess a wide bandgap energy (3-4 eV), which inhibits [12,4].

I-1-2-1 n-Type Transparent Conducting Oxides (n-TCOs) :

Definition: n-TCOs are materials that possess an excess of electrons in the conduction band.

Properties: n-TCOs exhibit high electrical conductivity, optical transparency, and chemical stability.

Applications: n-TCOs are utilized in applications such as touchscreens, solar cells, and electronic displays[12,5].

I-1-2-2p-Type Transparent Conducting Oxides (p-TCOs) :

Definition: p-TCOs are materials that possess an excess of holes in the valence band.

Properties: p-TCOs exhibit high electrical conductivity, optical transparency, and chemical stability.

Applications: p-TCOs are utilized in applications such as touchscreens, solar cells, and electronic displays[12,5].

I-1-2-3Differences between n-TCOs and p-TCOs :

Carrier Type: The primary difference between n-TCOs and p-TCOs is the type of charge carriers: electrons in n-TCOs and holes in p-TCOs.

Electrical and Optical Properties: The electrical and optical properties of n-TCOs and p-TCOs differ due to the difference in carrier type.

Applications: The applications of n-TCOs and p-TCOs differ due to the differences in properties and carrier type.

I-1-3Physical Properties of Transparent Conducting Oxides (TCOs):

I-1-3-1Electrical properties of TCOs:

- ***Bandgap Energy:***

The bandgap energy of Transparent Conducting Oxides (TCOs) is a critical parameter that influences their electrical and optical properties. The bandgap energy of TCOs is dependent on various factors, including the type of metal oxide, deposition method, and experimental conditions[12,6].

Table(I.1): Bandgap Energy Values of TCOs | TCO Material | Bandgap Energy (eV) |[12, 6].

TCO	Gap (eV)
ZTO	>3
ZnO	(3.2 - 3.3)
TiO2	(3 - 3.2)
SnO2	(3.6 - 4.2)
ITO	4.2

- ***Electrical Conductivity*:**

Definition and Units Electrical conductivity, denoted by σ (sigma), is a measure of the ability of a material to conduct electric current. It is defined as the ratio

of the current density to the electric field strength and is typically expressed in units of Siemens per centimeter (S/cm)[12,6].

Mathematical Representation The electrical conductivity of a material can be mathematically represented by the following equation:

$$\sigma = n * q * \mu \qquad (I\text{-}1)$$

where:

- **σ** (sigma) is the electrical conductivity
- **n** is the charge carrier concentration
- **q** is the elementary charge of an electron
- **μ** is the charge carrier mobility

➢ ***Surface Resistivity :***

Surface resistivity, denoted by Rs, is a measure of the resistance of a material to the flow of electric current along its surface. It is defined as the ratio of the resistivity of the material to its thickness and is typically expressed in units of ohms per square .

Mathematical Representation The surface resistivity of a material can be mathematically represented by the following equation[12,7]:

$$Rs = \rho / d \qquad (I\text{-}2)$$

where:

- **Rs:** is the surface resistivity
- **ρ**:is the resistivity of the material
- **d:** is the thickness of the material

➢ Electrical Mobility

The electrical mobility of charge carriers, including electrons and holes, is a crucial factor that influences the electrical conductivity phenomenon. An increase

in the mobility of charge carriers leads to an improvement in the electrical properties of transparent conducting oxides (TCOs). Dependence on Crystal Lattice The mobility of charge carriers primarily depends on their diffusion within the crystal lattice of the material. However, when the concentration of charge carriers increases significantly, the mobility value decreases due to collisions, resulting in reduced conductivity.

Mathematical Representation The relationship between mobility and conductivity is described by the following equation[12,7]:

$$\frac{q.I}{m*.vf} = \frac{q.\tau:}{m*} = \mu \qquad (I\text{-}3)$$

where:

q: Elementary charge of an electron, unit: C (Coulomb)

Vf: Fermi velocity of an electron

τ: Relaxation time (time between two successive collisions)

I: Mean free path (average distance traveled between two successive collisions)

m*: Effective mass of an electron

I-1-3-2Optical Properties of Transparent Conducting Oxides (TCOs):

The optical properties of TCOs are characterized by three fundamental phenomena: transmittance, reflectance, and absorbance. These phenomena are quantified by the following parameters: transmittance (T), reflectance (R), absorbance (A), and absorption coefficient (α)[12,8].

➢ Transmittance (T)

Transmittance is defined as the ratio of the transmitted light intensity (ΦT) . to the incident light intensity (Φ0) on the surface of the material. This parameter is a measure of the material's ability to allow light to pass through it[9].

$$T\%=100*T \quad (I\text{-}4) \quad \text{and} \quad T=\frac{\Phi T}{\Phi 0} \quad (I\text{-}5)$$

➢ Reflectance R:

Reflectance is defined as the ratio of reflected light intensity (ΦR) to incident light intensity (Φ0). Mathematically, it can be expressed as:

$$R = \Phi R / \Phi 0 \qquad (I\text{-}6)$$

The reflectance value is often expressed as a percentage:

$$R\,\% = (\Phi R / \Phi 0) \times 100 \qquad (I\text{-}7)$$

[9] .

➢ Absorbance A:

Absorbance is a measure of the amount of light absorbed by a material. It is defined as the ratio of absorbed light intensity to incident light intensity:

$$A = \Phi A / \Phi 0 \qquad (I\text{-}8) \text{ and } A\% = 100 * A \qquad (I\text{-}9)$$

where ΦA is the absorbed light intensity[9].

➢ Absorption Coefficient (α):

The absorption coefficient is a measure of the amount of light absorbed by a material per unit length. It is related to the absorbance by the following equation: $T = (1 - R) \exp(-\alpha d)$ where T is the transmittance, R is the reflectance, α is the absorption coefficient, and d is the thickness of the material.

Relationship Between Absorption Coefficient and Extinction Coefficient (K) The absorption coefficient is related to the extinction coefficient by the following equation: $\alpha = 4\pi K / \lambda$ where λ is the wavelength of light.

Determination of Optical Constants By measuring the transmittance, reflectance, and thickness of a TCO material, it is possible to determine its optical constants, including the refractive index, extinction coefficient, and bandgap energy[9].

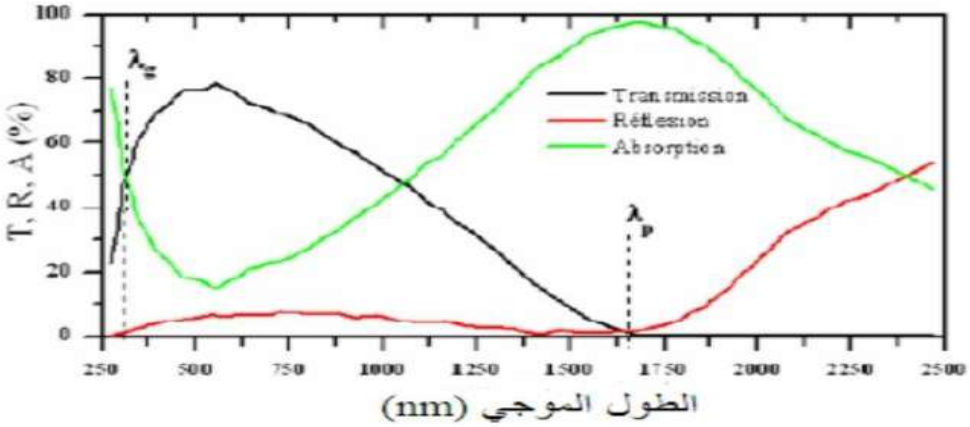

Figure (I.*1*): shows the evolution of transmittance, reflectance, and absorbance as a function of wavelength for a typical TCO material[10].

The reflectance and transmittance spectra of the TCO material, as reported by E.Elangovan et al., exhibit a limited range of wavelengths where the transmittance is minimal. This region can be referred to as the "optical window" due to the transparency of the material to electromagnetic radiation within this range. In the ultraviolet (UV) region, the photon energy exceeds the bandgap energy of the TCO material, resulting in the absorption of photons by electrons in the valence band, which then transition to the conduction band. The bandgap energy of TCOs varies between 3.6 and 4.3 eV, corresponding to photon wavelengths in the range of 300-400 nm (UV region). This energy is sufficient to promote electrons from the valence band to the conduction band. Within this spectral range, the bandgap energy (Eg) can be estimated. The optical properties of TCOs are crucial for understanding their behavior in various applications, including optoelectronic devices and solar cells.

- **Quality factor:**

properties of TCOs are intimately linked to their optical properties. In 1976, Haacke proposed a figure of merit (FOM) that correlates the electrical and optical properties of TCOs. This FOM is defined as the ratio of the average transmittance (T) in the visible region (400-800 nm) to the sheet resistance (Rs) of the TCO film[9].

Mathematically, the FOM can be expressed as:

$$\Phi_{Tc} = \frac{T^{10}}{R_{carree}} \qquad \text{(I-10)}$$

I-1-4Applications of Transparent Conducting Oxides (TCOs):

Transparent Conducting Oxides (TCOs) have a wide range of applications, including:

1. Solar Cells: TCOs are used as windows and anti-reflective coatings in solar cell systems.

2. Thermal Mirrors: TCO coatings on glass windows reduce thermal emissivity, minimizing heat transfer.

3. Light-Emitting Diodes (LEDs): TCOs are employed in LED manufacturing.

4. Gas Sensors: TCO-based sensors detect gas concentrations.

5. Surface Acoustic Wave (SAW) Devices: TCOs are used in SAW devices.

6. Ultrasonic Transducers: TCOs are employed in ultrasonic transducer technology.

7. Flat Panel Displays (FPDs): TCOs are essential components in the manufacture of flat panel displays, such as LCD TVs and computer monitors[11].

These applications leverage the unique combination of electrical conductivity and optical transparency offered by TCOs.

Figure (I.2):applications of Transparent Conducting Oxides (TCOs) [11]

I-2-Zinc Oxide (ZnO):

I-2-1-Definition:

wide-bandgap semiconductor belonging to the group (III-VI)family of transparent conducting oxides (TCOs). It exhibits natural n-type conductivity and crystallizes in the hexagonal wurtzite structure. Pure ZnO is a colorless, odorless powder that appears white or slightly yellowish in its solid form. Historical Background and Applications ZnO has been utilized as a white pigment for over two centuries due to its high reactivity and chemical stability. Its abundance and low cost make it an attractive material for transparent electrodes in thin-film solar cells[12].

Figure (I-3): Zinc oxide powder

I-2-2-2Properties of Zinc Oxide (ZnO):

Electrical Properties : Zinc oxide (ZnO) is a II-VI semiconductor material with a direct bandgap energy of 3.3 eV. The bandgap energy can vary depending on the doping level and preparation method, typically ranging from 3.0 to 3.9 eV. In practice, ZnO can be transformed into an n-type semiconductor through doping, resulting in high carrier concentrations of up to 10^20 cm^-3. Consequently, low resistivities of approximately 10^-2 Ωcm can be achieved in ZnO films. The electron mobility in thin-film ZnO typically ranges from 20 to 30 cm^2/Vs. In single-crystal ZnO, the maximum mobility reported is around 200 cm^2/Vs. The formation reaction of ZnO involves the following elements:

$Zn^{2+} + 2e^- + 1/2O_2 \rightarrow ZnO$

Property	Value
Direct bandgap energy	3.34 -/+ 0.02 eV
Minimum resistivity	$10^{-1}\Omega$cm
Maximum resistivity	$10^{-1}\ \Omega\ \mathrm{cm}$
Hole mobility	1.5
Electron mobility	
Density of states in valence (BV)	1.16 10^{19}
Density of states in conduction (BC)	3.71 10^{18}
Effective mass of electrons	0.24-0.28 me
Maximum electron drift velocity	2.2 10^{7}
Conductivity type	n type
Bandgap energy at 300K	3.34-/+ 0.02 eV
Bandgap energy at 4.2K	3.2 eV

Table(I.2): Electrical Properties of zinc oxide[13]

I-2-2-3Crystal Structure :

is a compound semiconductor material belonging to the group II-VI. Its ionic nature and position at the interface of covalent and ionic semiconductors make it a unique material. ZnO crystallizes in three main structures:

1. Zinc blende (B3)
2. Wurtzite (B4)

3. Rocksalt (B1)

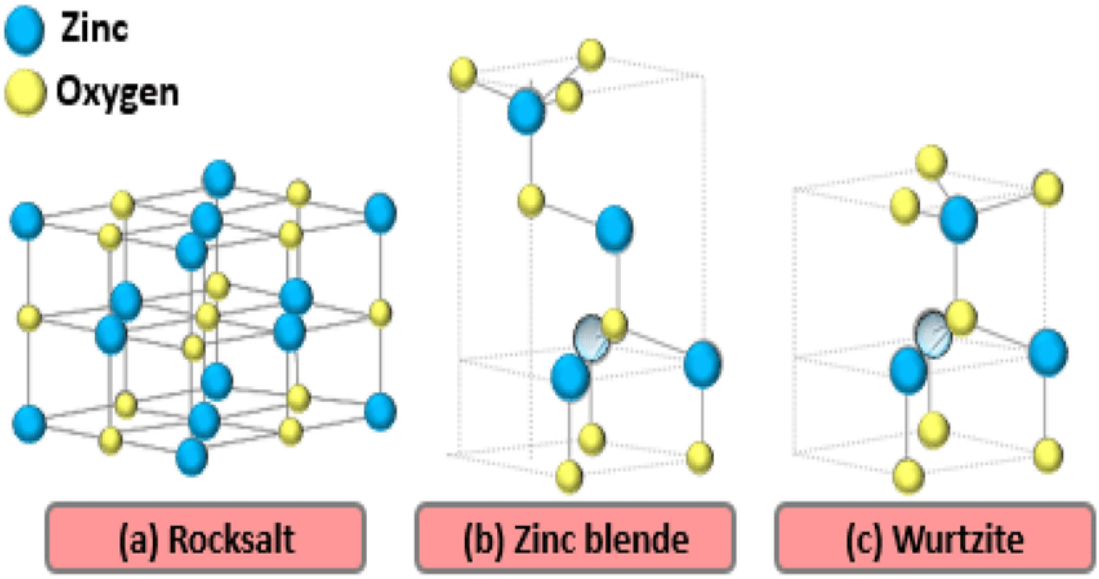

Figure (I.4):crystal structure representation[13]

the Wurtzite structure due to its high stability. The lattice constants of ZnO at room temperature (300 K) are a = 3.24958 Å and c = 5.20661 Å, with a c/a ratio of 1.633. The crystal density is approximately 5.65 g/cm³. The Wurtzite structure belongs to the space group P63mc and has a hexagonal primitive cell containing four atoms. The atomic positions are:

Zn: (0, 0, 0) and (1/3, 2/3, 1/2)

O: (0, 0, 1) and (1/3, 2/3, 1 + u)

where u is a dimensionless parameter that determines the position of the oxygen atom in the primitive cell along the [1010] direction. The value of u is given by: u = 0.375 - (8/3c/a - 2/3 - 1/8)

The Wurtzite structure is characterized by a tetrahedral coordination of zinc and oxygen atoms, with each zinc atom bonded to four oxygen atoms and each oxygen atom bonded to four zinc atoms[13].

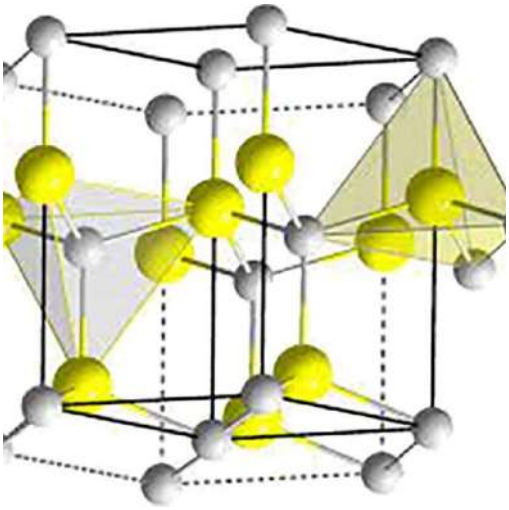

Figure(I.5) : hexagonal structure of (Zno)

I-2-2-4Physical and Chemical Properties of Zinc Oxide :

Table (I.3): The physical and chemical properties of zinc oxide (ZnO) are summarized

Property	**value**
Molecular weight (g/mol)	81.37
Melting point $(°C)$	1975
Boiling point $(°C)$	2360
Density(g/cm³)	5.67
Crystal structure	Hexagonal
Color	White
Refractive index	2.008

I-2-3Applications of Zinc Oxide (ZnO) :

Zinc oxide is a versatile material with unique properties and low cost due to its abundance in nature. As a result, ZnO has garnered significant attention and has numerous industrial and technological applications, including:

1. **Solar Cells**: ZnO is used as a transparent conducting oxide in solar cell devices.
2. **Gas Sensors**: ZnO-based sensors detect gas concentrations.

3. **Optical Waveguides**: ZnO is employed in the manufacture of optical waveguides.

4. **Thin-Film Coatings**: ZnO is used in the production of thin-film coatings, including anti-reflective coatings.

5. **Rubber and Tire Manufacturing**: ZnO is used in the production of rubber and tire manufacturing.

6. **Light-Emitting Diodes (LEDs)**: ZnO is used in the manufacture of LEDs.

7. **Variable Resistors**: ZnO is employed in the production of variable resistors.

8. **Glass Manufacturing**: ZnO is used in the production of glass[13;14].

I-3- copper oxide :

I-3-1Definition of Copper Oxide (CuO):

Copper oxide (CuO) is a semiconductor material with a p-type band structure. It is classified as a basic metal oxide and is typically found in the form of a fine powder with a dark brown to black coloration. CuO is odorless, non-toxic, and can be synthesized efficiently at a low cost. The material exhibits multiple oxidation states, but only two thermodynamically stable phases exist: CuO and Cu_2O[15] **.**

I-3-2Properties of Copper Oxide**:**

The table below summarizes the key physical and chemical properties of copper oxide (CuO)[16]:

Property	Value
Chemical formula	Cuo
Molar mass	79.545 g/mol
Density	6.315 g/cm³
Color	Brown or green
Melting point	1326 °C
Boiling point	2000°C
Solubility	Insoluble in water and alcohol ;soluble in ammonium chloride
Bandgap energy(Eg)	1.2 eV
Lattice parameters	a=4.6837 Å, b=3.4226 Å , c=5.1288Å
Refractive index	2.63
Crystalline structure	Monoclinic

Table(I.4): the key physical and chemical properties of copper oxide (CuO)[16]

I-3-3Applications of Copper Oxide:

Copperoxide has attracted significant attention in recent years due to its unique properties and wide-ranging applications across various fields. These applications include:

Photovoltaic cells: Used in solar energy conversion.

Electrical circuit manufacturing: Used in the production of electronic circuit boards as a key component of electrical conductors.

Gas sensors: Utilized in environmental and industrial monitoring systems[17].

[1] ن. محمد علي الكرخي دراسة الخصائص التركيبية و البصرية لاغشية **(Zno:Sn)** المحضرة *بطريقة التحلل الكميائي الحراري رسالة ماجستير جامعة ديالي العراق 2012*

[2] زينب أولاد العربي - سهام القريدة - تأثير التطعيم الثنائي بالفلور والكوبالت على خصائص البنيوية والضوئية والكهربائية للاغشية الرقيقة لاكسيد الزنك مرسبة بتقنية رذاذ الانحلال الحراري _ فيزياء الاشعاعات - جامعة قاصدي مرباح ورقلة 2020.

[3]فرج الله منال - تحضير ودراسة تاثير تطعيم أكسيد القصدير Sno2 على بعض الخصائص الفيزيائية - مذكرة ماستر اكاديمي - فيزياء طاقوية طاقات متجددة _ جامعة محمد خيضر بسكرة 2022

[4]نقودي نيرمان _ دراسة خصائص البنيوية والكهربائية والضوئية لاغشية أكسيد القصدير

[5]دروج ش خديري. سمية _ تحضير ودراسة الشرائح الرقيقة لاكسيد الزنك ZnO بدلالة التركيز وعدد طبقات فيزياء الطاقة والطاقات المتجددة جامعة محمد خيضر بسكرة 2020.

[6]محمدي ع القادر - دراسة الطبقات ذات الخصوصية اللغوية - فيزياء تطبيقية - جامعة محمد بوضياف المسيلة 2017.

[7]طيب ارفيس _ خصائص البنيوية والضوئية للطبقات الرقيقة لاكسيد الزنك المطعم بذرات النيكل والمحضرة بطريقة الطرد المركزي - فيزياء تطبيقية - جامعة محمد بوضياف المسيلة 2018

[8]محمدي عبد القادر - دراسة الطبقات الرقيقة ذات الخصوصية اللغوية - فيزياء تطبيقية - جامعة محمد بوضياف المسيلة 2017

[9]بن عمر ساره – دراسة الخواص الفيزيائية للطبقات الرقيقة لاكسيد الزنك المطعم بالحديد المتوضع بتقنية رذاذ الانحلال الحراري –فيزياء المواد – جامعة قاصدي مرباح ورقلة 2016

[10]E. Elangovan, Applied Surface Science, A study on low cost-high conducting fluorine and antimony-doped tin oxide thin films, Vol. 249,N.1-4, 2005 183- 196.

[11] جهينة بوصبيع صالح –صفاء لبيهات-دراسة الخصائص التركيبية و البصرية لاغشية اكسيد النيكل المطعمة بالنحاس –فيزياء تطبيقية –جامعة الشهيد حمه لخضر بالوادي -2018

[12] بالهاني سمية-تحضير و معاينة الطبقات الرقيقة من اكسيد الزنك المطعم بالمغنيزيوم و اختبار اداءها في التحفيز الضوئي

[13]فطيمي مريم – خرفي هاجر –الدراسة النظرية لانابيب النانوية لاكسيد الزنك –فيزياء المواد –جامعة قاصدي مرباح ورقلة 2022

[14] A. Rahal Elaboration des verres conducteurs par dèposition de ZnO sur des verres ordinaires universitè d´ EL oued.2013.p1.

[15]مزنر امينة –تحضير مسحوق اكسيد الزنك بابعاد نانومترية و اختبار نشاط التحفيز الضوئي له –فيزياء المواد -الجامعة محمد الصديق بن يحي جيجل 2022

[16]M.LAMRIZEGGAR –Cuprie oxide thin films deposition for gaz senor application –universite FERES-MENTOURI Constantine-1-2016

[17]A.BEJAOUI *Capteurs à base des couches mince d´ oxyde de cuivre : Optimisation et modèlisation en vue de la dètection de gaz-universitè Aix Marseille et universitè carthage ,2013

Chapter2:Thin film deposition and analysis methods

Introduction :

Thin films of zinc oxide (ZnO) have attracted significant attention due to their promising optical and electronic properties. Among various deposition techniques, ZnO films prepared using the sol-gel method have demonstrated remarkable performance, particularly when spin coating is applied[1].

These films exhibit superior uniformity, optical transmittance, and adherence to the substrate, making them ideal candidates for applications in optoelectronic devices, transparent conductive oxides, sensors, and photovoltaic cells. Studies have shown that specific orientations of ZnO nanostructures can result in enhanced transparency and photoluminescence, depending on the processing conditions and substrate material[1].

In this chapter, we will explore the fundamental concepts of thin films and their significance in modern material science. We will also discuss the physical and chemical mechanisms involved in their formation, with a focus on the sol-gel spin coating technique as our primary synthesis method. Additionally, we will cover the step-by-step process of film preparation, including precursor preparation, deposition parameters, drying, and annealing. The chapter will also address various characterization techniques used to analyze the structural, morphological, optical, and electrical properties of the deposited ZnO thin films [1]

II-1Defintion of thin films:

Thin films refer to layers of material with thicknesses ranging from a few nanometers to several micrometers, resulting from the condensation of atoms or molecules on a substrate. These films exhibit unique physical and chemical properties that differ from those of the bulk material due to surface effects. The substrate's structure and properties significantly influence the film's structural and physical characteristics [2,12].

II-2principles of thin film deposition :

The deposition of thin films involves the transfer of particles (atoms, molecules, or ions) through a medium (gas, liquid, or solid) onto a substrate. The particles

interact with the substrate surface through van der Waals forces or chemical reactions. The choice of medium and deposition method significantly affects the film's properties[3].

- Liquid Medium:

  This method is widely used due to its simplicity and versatility. Techniques such as sol-gel deposition and chemical bath deposition are commonly employed[2].

- Deposition Methods in Gaseous or Vacuum Environments:

  Deposition techniques in gaseous or vacuum environments involve chemical vapor deposition (CVD) methods. The primary distinction between gaseous and vacuum environments lies in the mean free path of the molecules, which affects the deposition process[2].

II-3 Stages of Thin Film Deposition:

The deposition of thin films is a complex process that requires careful control of several stages. To achieve the desired film properties, it is essential to follow specific experimental conditions due to the high sensitivity of the microstructure. The process typically consists of three key stages[1]**:**

1. Preparation of Deposition Materials The materials to be deposited are prepared in the form of ions, molecules, or atoms, often in a solution or precursor form. This stage is crucial in determining the chemical composition and purity of the deposited film[1].

2. Transport of Deposition Materials The prepared materials are then transported to the substrate, which can be achieved through various methods, such as vapor phase transport or liquid phase transport[1].

3. Condensation on the Substrate The materials are condensed onto the substrate, typically made of glass or other materials, either directly or through chemical reactions, resulting in the formation of a solid deposit[1].

The process of thin film formation involves three distinct stages: nucleation, coalescence, and growth.

II-3-1 Nucleation Stage:

In the nucleation stage, small clusters of atoms or molecules form on the substrate surface. These clusters undergo transformations in their material state, resulting in the formation of a new physical and chemical structure. The interaction between the atoms or molecules and the substrate surface leads to the formation of nuclei, which serve as the foundation for further growth[4].

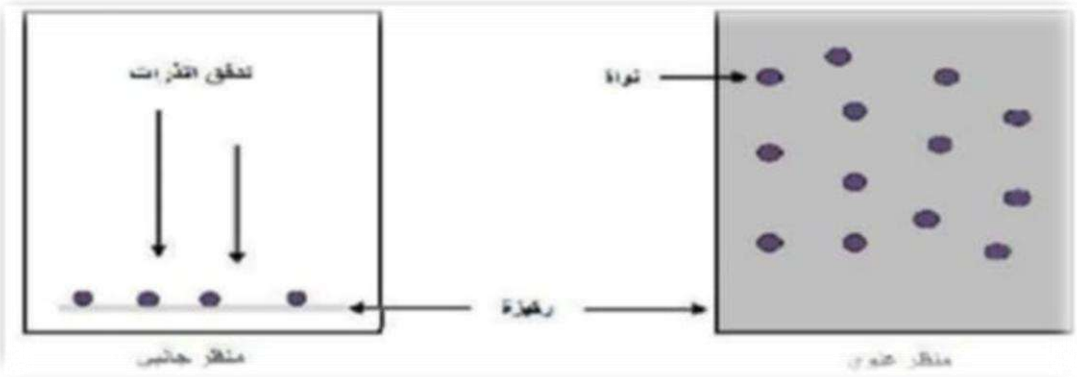

Figure(II-1): illustrates a schematic diagram of the atomic arrangement phase [35]

II-3-2 Coalescence Stage:

As the nuclei grow in size, they begin to merge with each other, forming islands on the substrate surface. This stage is characterized by the coalescence of the islands, leading to the formation of a continuous film[4].

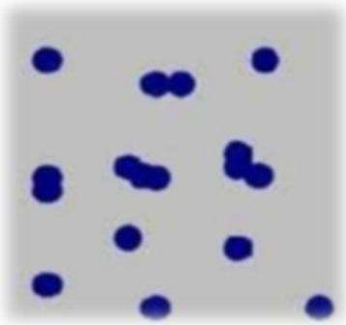

Figure(II-2): depicts the coalescence stage between the nuclei [35]

II-3-3 Growth Stage: The final stage of thin film formation is the growth stage, where the islands continue to grow and merge, forming a continuous film with a specific microstructure. The film's microstructure is influenced by the growth mode, which can be classified into three primary modes:

Frank-Van der Merwe (2D) Growth Mode: This mode involves layer-by-layer growth, where atoms are deposited uniformly on the substrate surface. **Volmer-Weber (3D) Growth Mode**: This mode involves columnar growth, where atoms are deposited non-uniformly on the substrate surface. **Stranski-Krastanov Growth Mode**: This mode is a combination of 2D and 3D growth modes, where the film grows layer-by-layer initially, followed by island formation[4].

Figure(II-3):shows the growth patterns of thin films [35]

II-4Methods of Thin Film Deposition:

Various techniques are employed in the field of thin film fabrication, owing to the wide range of applications and the diversity of thin film types.

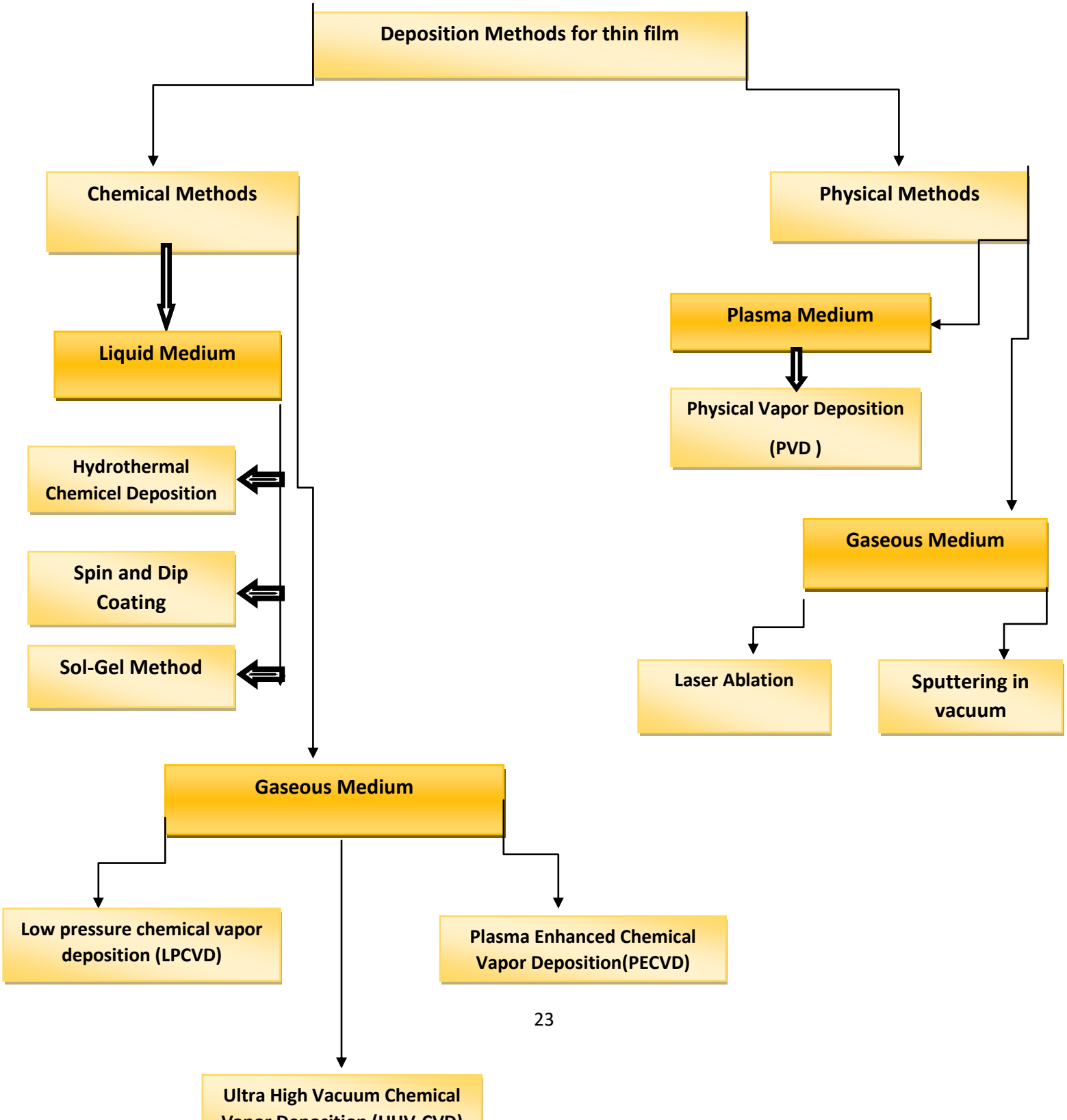
Deposition Methods for thin film
Chemical Methods
Physical Methods
Liquid Medium
Plasma Medium
Physical Vapor Deposition (PVD)
Hydrothermal Chemicel Deposition
Spin and Dip Coating
Sol-Gel Method
Gaseous Medium
Laser Ablation
Sputtering in vacuum
Gaseous Medium
Low pressure chemical vapor deposition (LPCVD)
Plasma Enhanced Chemical Vapor Deposition(PECVD)
Ultra High Vacuum Chemical

Figure (II.4): shows various techniques for thin film deposition.

II-4-1 Chemical Methods for Thin Film Deposition:

II-4-1-1 Chemical Vapor Deposition (CVD):

CVD is a method that enables the formation of a thin film on a substrate through chemical reactions between gases and the substrate surface. This process requires a substrate temperature above 300°C to provide the necessary activation energy for the chemical reaction. The deposition process is influenced by factors such as substrate nature and temperature, chemical composition of the starting materials, gas flow, and total pressure. CVD is widely used in various fields, including the fabrication of semiconductor devices. However, the high temperatures required for CVD can be a limitation. To address this, several modifications have been developed, including[5,6,]:

- Plasma-Assisted CVD (PACVD):

This method uses plasma to activate the chemical reaction, allowing for deposition at relatively low temperatures (<300°C). However, the plasma can react with the substrate, resulting in non-uniform films[7].

- Low-Pressure CVD (LPCVD): This method involves chemical reactions under low pressure (10^-3 - 10^-1 Torr) [8,9].

- Ultra-High Vacuum CVD (UHV-CVD): This method involves depositing thin films under pressures below 10^-12 Torr[8].

II-4-1-2Sol-Gel Technique:

The sol-gel technique has been known for over 150 years, dating back to the work of Ebelmen. This method has been significantly developed over the past few decades. Starting from a solution composed of reactants dissolved in an alcohol, thin films can be formed using two methods[10]:

- Spin coating: Spin coating involves depositing a solution onto a substrate, which is then rotated at a controlled speed to form a uniform film. The thickness is determined by the rotation speed and the properties of the solution[11] .

- Dip coating: Dip coating is a technique where a substrate is immersed in a solution, allowing a thin film to form on its surface. The thickness of the film is influenced by the vertical speed of the substrate withdrawal. This method provides a simple and cost-effective way to deposit thin films[11].

The sol-gel technique offers a versatile method for depositing thin films with controlled composition and microstructure.

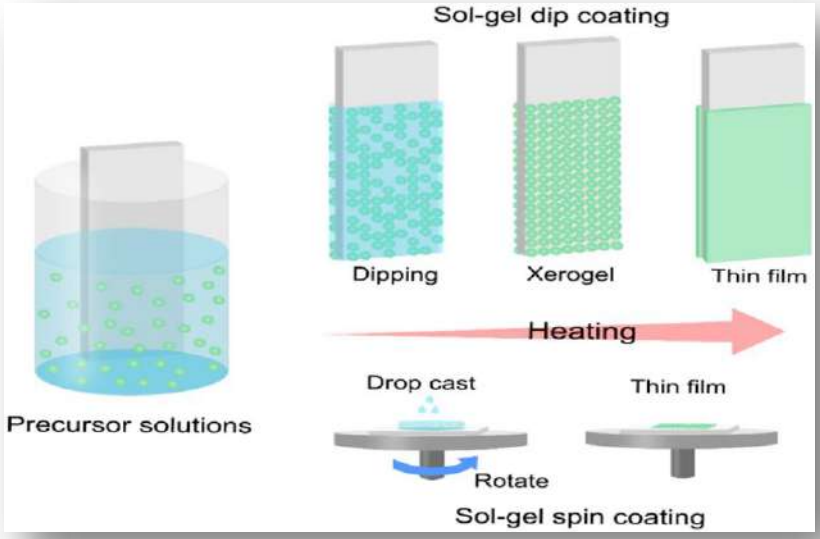

Figure (II.5): Schematic diagram showing the dip coating and spin coating deposition techniques.

Advantages of this Technique:

The advantages of this technique include[12]:

- Low temperatures used during the preparation of thin films
- Precise control over the reacting elements

- High purity of the resulting thin films

Disadvantages of this Technique:

The disadvantages of this technique include

- The technique is somewhat chemically complex[13].

II-4-1-3 Ultrasonic Spray Pyrolysis Method (Physical Method): The ultrasonic spray pyrolysis method relies on utilizing the energy of ultrasonic waves through a generator operating at high frequencies (40 kHz). This allows the solution to be converted into fine droplets with diameters of 40 micrometers, which are then sprayed onto a heated substrate at temperatures ranging from 250 to 500°C. This process activates the chemical reaction between the components, and unwanted reaction products (volatile elements) are immediately removed, leaving only the desired compound (e.g., zinc oxide) deposited on the substrate [14].

Figure (II.6): Ultrasonic Spray Pyrolysis Technique

II-4-2 Physical Methods:

II-4-2-1Physical Vapor Deposition (PVD):

The Physical Vapor Deposition (PVD) technique relies on the thermal evaporation process of materials under low pressure. It has several advantages compared to

the Chemical Vapor Deposition (CVD) method, as it is considered a non-polluting technique, and the deposited layer is dense and easy to monitor. Among the most commonly used PVD methods are evaporation under vacuum, sputtering, and pulsed laser deposition[15].

II-4-2-2 Evaporation in Vacuum:

This technique relies on the evaporation or sublimation of the material to be deposited by heating it to high temperatures. This process occurs inside a vacuum chamber, and the evaporated material is deposited on the substrate through condensation, forming a thin layer on its surface. The heating methods vary, including resistive heating or using a high-energy electron beam (5-...). The first method is used for materials with low melting points, while the second method is used for refractory materials. The deposition rate depends on the source temperature and the distance between the evaporated material and the substrate[16].

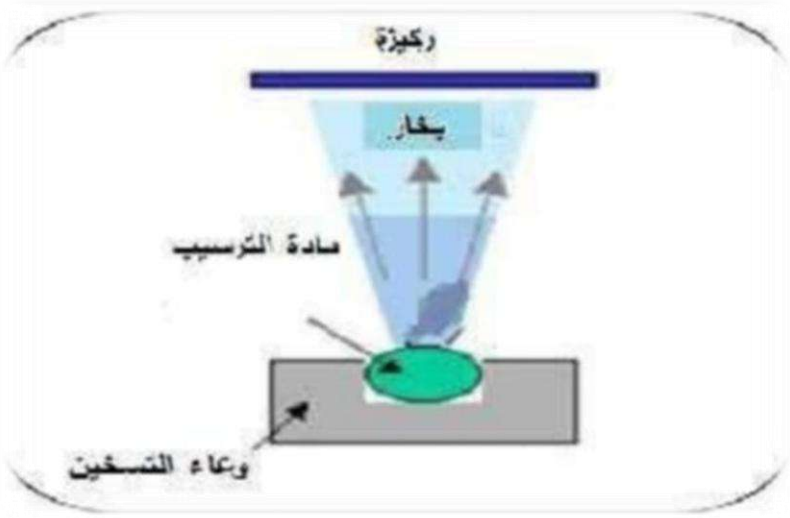

Figure (II-7): Evaporation Method in Vacuum[36]

II-4-2-3 Sputtering:

In this method, the substrate is placed inside a chamber containing a gas (usually argon) at low pressure. The low pressure causes a discharge, which plays a role in ionizing the gas atoms. The resulting ions are accelerated by a potential difference

to collide with the cathode. The cathode is made of the material to be deposited, also known as the target[17,20].

Under the impact of the accelerated gas ions, atoms are ejected from the cathode and deposited onto the substrate surface. In some cases, a second gas is introduced in addition to argon, which reacts chemically with the ejected atoms to form desired compounds that deposit on the substrate. The advantages of this method include[18]:

- Deposition under controlled atmospheres[18].

The disadvantages include:

- High setup costs for the sputtering device.
- Slow deposition rate[19].

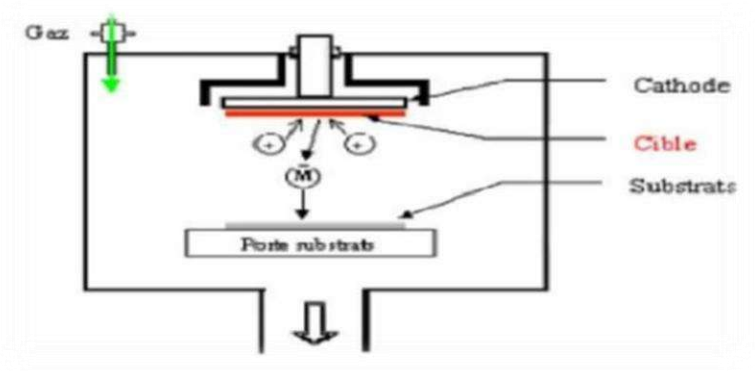

Figure (II-8) : Schematic diagram of the sputtering technique[18]

II-4-2-4 Pulsed Laser Deposition (PLD) :

Pulsed Laser Deposition (PLD) is a technique that involves directing a high-intensity laser beam onto a target made of the material to be deposited. The target is larger than the laser beam, and the laser power is sufficient to eject a quantity of material from the target. The ejected material forms a plume that is perpendicular to the target surface and deposits onto a heated substrate. The substrate is placed parallel to the target, as shown in Figure (I-9), to provide the necessary energy for crystallization of the thin film[18].

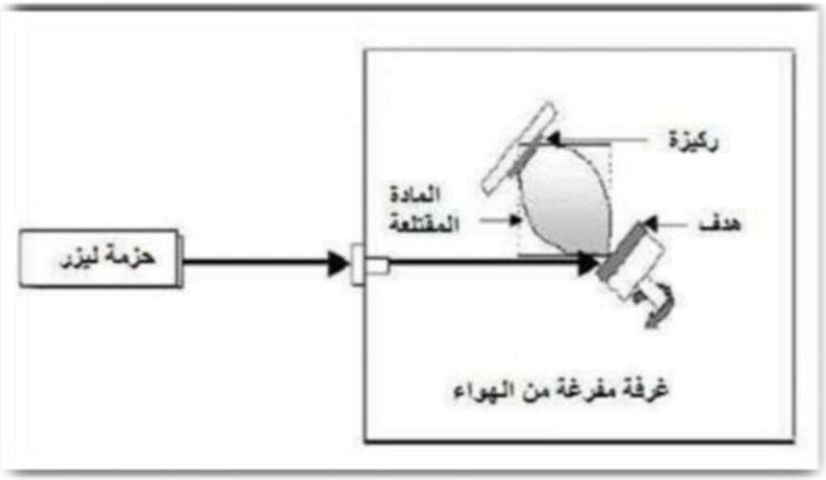

Figure(II-9): A schematic diagram illustrating the deposition process using Pulsed Laser Deposition (PLD) technique[11].

II-5-1Structural Properties:

The study of structural properties of thin films contributes to determining the identity of the obtained films, including their nature, crystal structure, and type of crystalline planes. Investigating structural properties helps interpret the diverse and numerous results obtained due to variations in preparation conditions, doping materials, and other factors. The crystalline structure of a material is typically determined using one of the various X-ray diffraction (XRD) techniques [21].

II-5-1-1 X-Ray Diffraction (XRD):

XRD is a technique used to determine the crystalline structure, lattice parameters, and preferred orientation of thin films prepared under specific conditions, as well as to study their atomic arrangement. X-rays were discovered by Wilhelm Conrad Röntgen in 1895, and since then, the field has developed extensively, enabling the determination of atomic structures. The use of X-rays has expanded to various fields, and in 1912, Max von Laue demonstrated the diffraction of X-rays by crystals, allowing for the determination of interatomic distances using XRD. This technique has become a crucial tool for analyzing the structural properties of materials.

This method relies on exposing the sample to monochromatic X-rays. A portion of these X-rays is reflected by the atomic planes of the crystal in specific directions

and with varying intensities, depending on the orientation and number of planes. The intensity of the reflected X-rays is recorded as a function of the deviation angle (2θ) of the beam, as shown in Figure (II-10) [1].

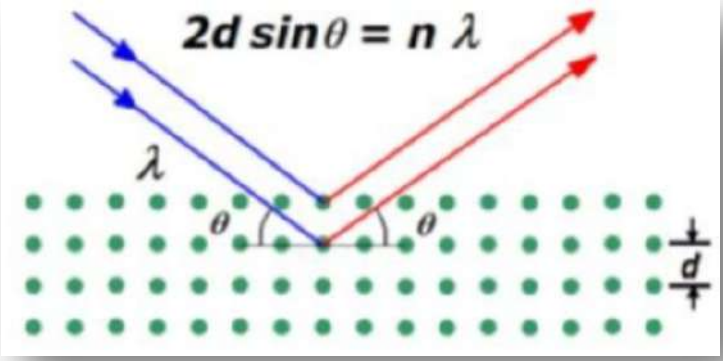

Figure(II-10): A diagram showing X-ray diffraction on crystal planes[1].

II-5-1-2 Principle of X-Ray Diffraction:

When a monochromatic X-ray beam is directed towards a polycrystalline sample, a portion of the beam is reflected by the atomic planes in the crystals in specific directions and with varying intensities, depending on the orientation and number of planes. In reality, the reflected waves from the same family of planes interfere constructively with each other and are then measured by a detector[3].

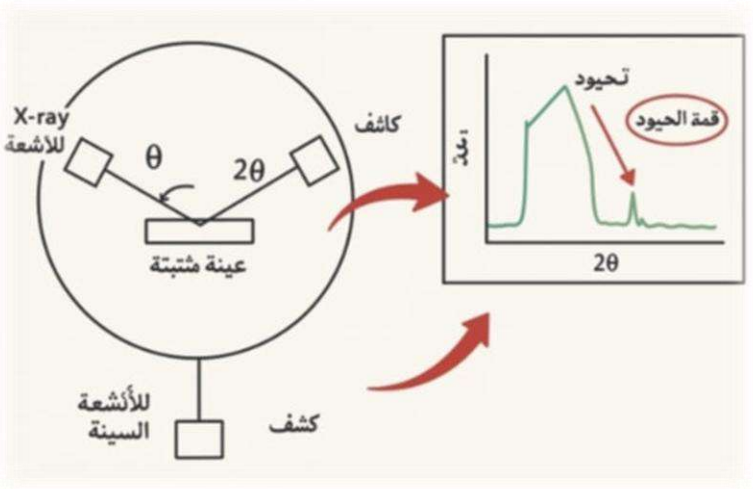

Figure(II-11): A schematic diagram illustrating the mechanism of X-ray diffraction.

II-5-1-3 Bragg's Law and X-Ray Diffraction:

Bragg's Law, discovered by William Henry Bragg and William Lawrence Bragg in 1913, describes the diffraction of X-rays by crystals. When a monochromatic X-ray beam is incident on a crystal at a specific angle, it is diffracted, producing a diffraction pattern with maxima of intensity. These maxima are known as Bragg reflections[22].

Mathematical Formulation of Bragg's Law The mathematical formulation of Bragg's Law is given by:

$$n\lambda = 2d \sin(\theta) \quad (II\text{-}1)$$

where:

n = order of diffraction (integer)

λ = wavelength of X-rays

d = interplanar spacing between crystal planes

θ = angle of diffraction

II-5-1-4X-Ray Diffraction Device:

An X-ray diffraction device consists of a sample holder, an X-ray detector, and a goniometer that measures the angle of diffraction. The X-rays emitted from the source are diffracted by the sample, and the detector measures the diffracted radiation as a function of the angle (2θ). The resulting diffraction pattern is represented as a diffractogram, which plots the intensity of the diffracted photons against the angle (2θ) [23].

Figure(II-12): X-ray diffraction device DRX

II-5-1-5Determination of Structural Properties using X-Ray Diffraction:

Knowledge of the structural factors of a material, which can be determined using X-ray diffraction (XRD) patterns, is crucial in understanding many of its physical properties. For materials with a hexagonal structure, such as ZnO, the lattice parameters (a and c) can be calculated using the XRD pattern. Calculation of Lattice Parameters The lattice parameters a and c can be calculated using the following formulas[1]:

$$\frac{1}{dhkl^2} = \frac{3}{4}\left(\frac{h^2+hk+k^2}{a^2}\right) + \frac{l^2}{c^2} \qquad \textbf{(II-2)}$$

a =

$$\frac{\lambda}{\sqrt{3}\sin o\ (100)} = \frac{2*d100}{\sqrt{3}} \qquad \textbf{(II-3)}$$

$$c=\frac{\lambda}{\sin o\ (002)} = 2 * d002 \qquad \textbf{(II-4)}$$

where λ is the wavelength of the X-rays, and θ is the Bragg angle.

Calculation of Crystallite Size The crystallite size: can be calculated using the Scherrer equation, which relates the crystallite size to the broadening of the diffraction peaks. The equation is given by[24]:

$$Cs = \frac{K\lambda}{\beta \cos(\theta)} \qquad (II\text{-}5)$$

Where:

Cs :is the crystallite size,

K: is a constant (typically 0.9),

λ: is the wavelength of the X-rays,

β :is the full width at half maximum (FWHM) of the peak

θ :is the Bragg angle.

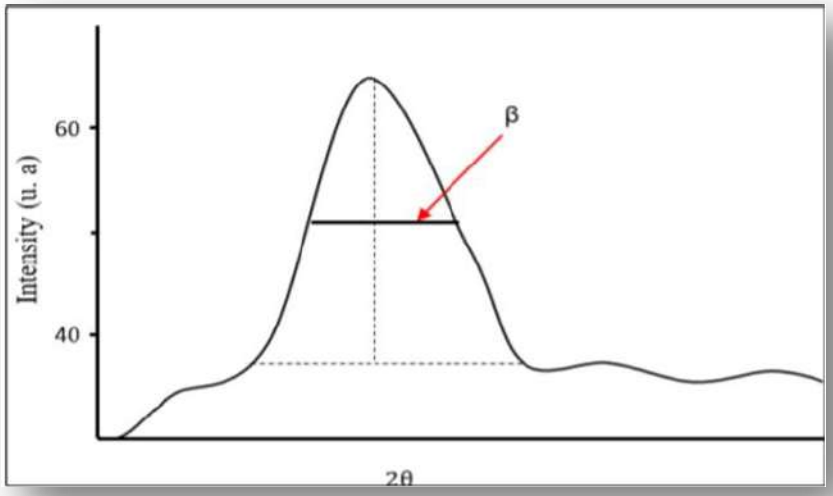

Figure(II-13): Method for determining the full width at half maximum [37].

II-5-2Optical Properties:

UV-Vis Spectroscopy The study of optical properties using spectroscopic analysis allows for the description of various characteristic constants of thin films. Optical methods are preferred over electrical methods due to their non-destructive and sensitive nature. UV-Vis spectroscopy is a technique that involves the interaction of light with a sample, resulting in the absorption or transmission of light[25].

II-5-2-1Ultraviolet (UV) Radiation:

UV radiation is a type of non-ionizing electromagnetic radiation with wavelengths ranging from 200-400 nm. It is divided into three categories[25]:

- UVA (320-400 nm): longest wavelength, least energy
- UVB (290-320 nm): medium wavelength, moderate energy
- UVC (200-290 nm): shortest wavelength, highest energy [26]

Principle of UV-Vis Spectroscopy:

The principle of UV-Vis spectroscopy is based on the interaction between light and the sample, resulting in the absorption or transmission of light. When a material absorbs light in the UV-Vis range, it causes electronic transitions from lower to higher energy levels. These transitions occur in the visible (200-800 nm) and UV (200-350 nm) ranges.

Instrumentation: A UV-Vis spectrophotometer consists of a light source, typically a combination of tungsten and deuterium lamps. The deuterium lamp emits wavelengths from 180-400 nm (UV range), while the tungsten lamp emits wavelengths from 400-800 nm (visible range) [27].

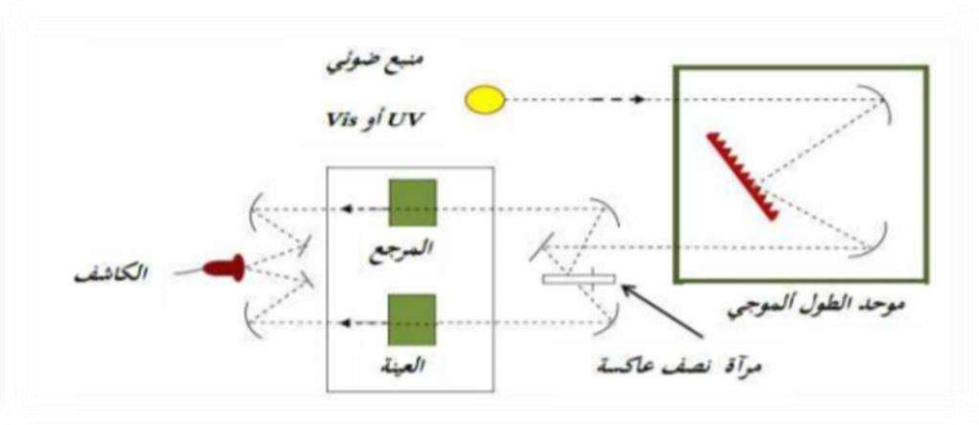

Figure(II-14): schematic diagram of ultraviolet – visible spectroscopy [1]

Figure(II-15): ultraviolet-visible spectrophotometer

Determination of Material Properties using UV-Vis Spectroscopy The UV-Vis spectroscopy results for the thin film were analyzed to plot the transmittance curves as a function of wavelength in the UV-Vis range. These curves provide valuable information on the material's properties, which can be extracted and utilized for further analysis and characterization.

- **Determination of Absorption Coefficient α**:

The absorption coefficient (α) can be determined from the transmittance spectrum using the Lambert-Beer law, which is given by the equation [28]:

$$T = \exp(-\alpha d) \qquad (II\text{-}6)$$

where

T: is the transmittance

α: is the absorption coefficient

d: is the thickness of the layer.

By rearranging this equation, the absorption coefficient can be calculated as:

$$\alpha = \frac{1}{d} ln \frac{100}{T\%} \qquad (II\text{-}7)$$

- **Determination of Bandgap Energy:**

The bandgap energy (Eg) is defined as the energy required to transfer electrons from the top of the valence band to the bottom of the conduction band. The

relationship between the absorption coefficient and the bandgap energy is given by the Tauc equation [29]:

$$(\alpha\, h\nu)2=(h\nu-Eg) \quad (II\text{-}8)$$

Where:

Hv: is the energy of the incident photon

B: is a constant

. By plotting $(\alpha h\nu)^2$against hv, the bandgap energy can be determined from the intercept of the linear portion of the curve with the energy axis.

Analysis and Results By analyzing the transmittance spectrum and plotting (αhv) against hv, the bandgap energy of the material can be determined.

This information is crucial in understanding the electronic properties of the material and its potential applications[30].

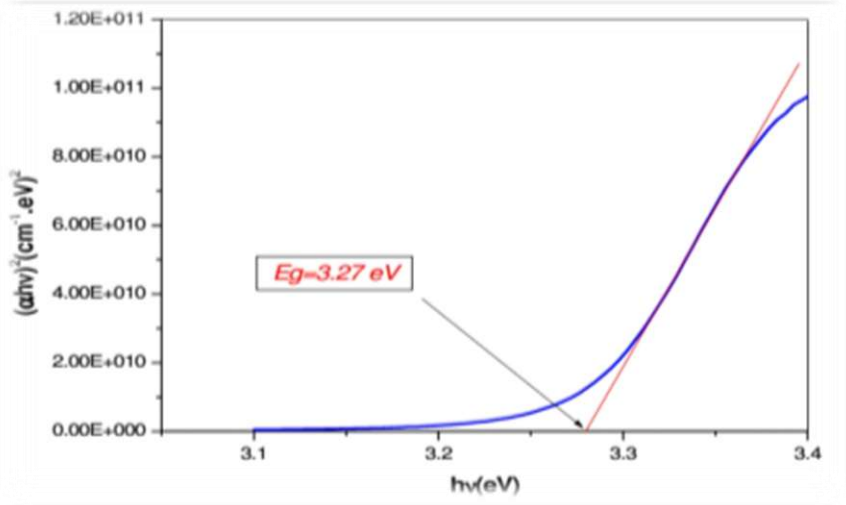

Figure(II-16): plot of $(\alpha h\nu)^2$ versus (hv) [1]

The bandgap energy (Eg) can be determined by extrapolating the linear portion of the $(\alpha h\nu)^2$ vs. hv curve to the energy axis. The point of intersection represents the value of Eg.

II-5-3 Morphological Properties:

II-5-3-1Scanning Electron Microscopy (SEM):

SEM is a technique that produces an image of the surface of a sample by scanning it with a focused electron beam. This technique is based on the principle of electron-matter interactions and is capable of providing high-resolution images of the sample surface. The SEM image is formed by detecting the signals emitted from the sample, including secondary electrons, backscattered electrons, and X-rays [32].

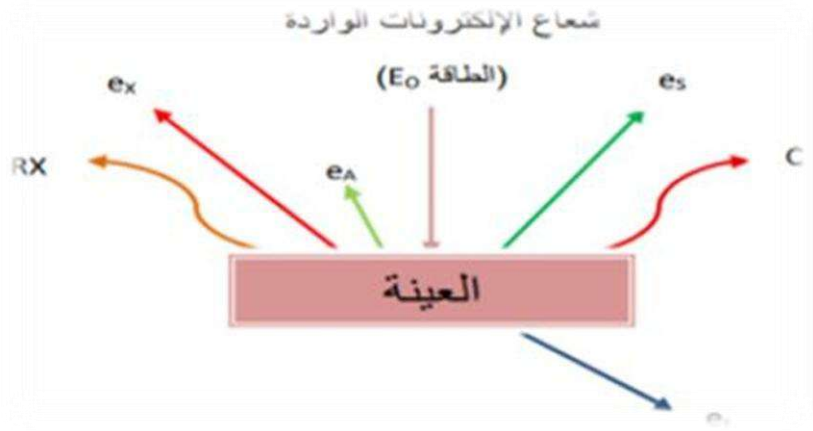

Figure(II-17): Illustrates the interactions of the electron beam incident on the sample[1]

The principle of SEM is based on the interaction of the electron beam with the material, where a focused electron beam is scanned across the sample surface. The electron beam is concentrated and condensed through two stages of focusing, resulting in a beam diameter of a few nanometers, effectively acting as a "probe" to scan the sample.

The SEM operates by scanning the sample surface in a raster pattern, from bottom to top and left to right, collecting and counting the emitted signals from each point on the sample. These signals are then used to generate an image, with each pixel corresponding to a specific point on the sample surface, and assigned a grayscale value based on the intensity of the signal[33].

Advantages of SEM: SEM is a highly advanced imaging technique that provides a comprehensive view of the sample surface, offering detailed information on the

morphology, topography, and composition of the material. The high-resolution images obtained through SEM enable researchers to gain valuable insights into the material's properties and behavior.

Figure(II-18): Scanning Electron Microscope (SEM)

II-2-3-5 Photocatalysis:

The term "photocatalysis" is derived from two components: the first, "photo," refers to light, while the second, "catalysis," refers to the acceleration of a chemical reaction. Photocatalysis involves a chemical process in which light is used to activate a material (acting as a catalyst) that enhances the reaction rate without itself undergoing permanent change [1].

The photocatalytic process occurs when a semiconductor (SC) is exposed to light energy equal to or greater than its band gap. The absorbed energy excites electrons from the valence band to the conduction band, leaving behind positive holes. These charge carriers (electrons e^- and holes h^+) migrate to the surface of the semiconductor, where they can participate in redox reactions. These reactions may include the oxidation of organic compounds or the reduction of other species. The efficiency of this process is influenced by the potential for recombination of charge carriers. However, the presence of co-catalysts or

suitable materials on or near the semiconductor surface can enhance the separation of these charges. For instance, materials with high electron affinity (A) and electron donors (D) in close contact with the semiconductor can significantly improve photocatalytic efficiency by preventing recombination and extending the lifetime of charge carriers, thus allowing for a sequence of effective photocatalytic reactions [32].

Upon absorbing sufficient light energy, a semiconductor (SC) can generate an electron-hole pair (e^-/h^+). These charge carriers may recombine (recombination), or they may participate in separate redox reactions at the surface of the semiconductor.

The basic photoexcitation process can be represented as:

$$\mathbf{SC + h\theta \rightarrow e^-}$$

The generated holes can react with water to form hydroxyl radicals (OH*), which are highly reactive:

$$\mathbf{HO_2 + h^+ \rightarrow OH^{*-} + H}$$

Similarly, electron donors (D) can undergo oxidation directly by the holes:4

$$\mathbf{D + h^+ \rightarrow D^{*+}}$$

On the other hand, the photogenerated electrons may reduce electron acceptors (A) or oxygen molecules:

$$\mathbf{A + e^- \rightarrow A^{*-}}$$

$$\mathbf{O_2 + e^- \rightarrow O_2^{*-}}$$

II-4-5 Membrane Thickness Measurement:

Measuring membrane thickness is critical, as it is one of the key parameters for thin films. Several methods exist for this purpose; in our study, we rely on the

gravimetric method. This involves weighing the glass substrate before and after the deposition using a highly sensitive digital balance[33].

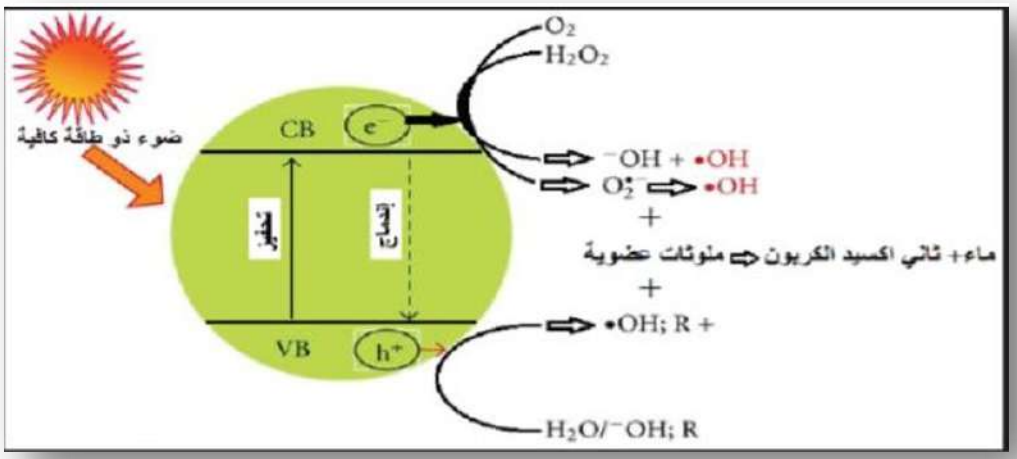

Figure(II-19): Schematic diagram of the mechanism of heterogeneous photocatalysis in semiconductors[25]

The membrane thickness is then calculated using the following equation:

$$d = \frac{\Delta m}{\rho . s} \qquad \textbf{(II-9)}$$

Where:

- d: membrane thickness (cm)
- Δm: mass difference (weight of the deposited film)
- ρ: density of the deposited material (g/cm³)
- s: surface area of the substrate (cm²)

[1]بالهاني سمية-تحضير و معاينة الطبقات الرقيقة من اكسيد الزنك المطعم بالمغنيزيوم و اختبار اداءها في التحفيز الضوئي

[2]جهينة بوصبيع صالح –صفاء لبيهات-دراسة الخصائص التركيبية و البصرية لاغشية اكسيد النيكل المطعمة بالنحاس –فيزياء تطبيقية –جامعة الشهيد حمه لخضر بالوادي -2018

[3]ح بن سالم دراسة الخصائص البنيوية والكهربائية والضوئية لشرائح أكسيد القصدير Sno مطعم بالانتموان Sb موضع بطريقة الأمواج فوق الصوتية، مذكرة ماستر أكاديمي جامعة الوادي 2014.

[4] A.Necmeddin Yazici , O. Mustafa ztas – MetinBed ir , Journal of Lumminescence 104 (2003) 115 .

[5] A. Hafdallah, Etude du Dopage des Couches Minces de ZnO Elaborées par Spray Ultrasonique, thème de magister, université de Constantine, 2007.

[6] A. MOUSTAGHFIR, laboration et caractérisation de couches minces d'oxyde de zinc, université BLAISE PASCAL., p19, (novembre 2004).

[7] S. Menakh, Contribution à l'Etude des Propriétés de Films ZnO, thème de magister, université de Constantine, 2010.

[8] L. B. Freund, S. Suresh. Matériaux en couches minces : Sten, formation de défauts et évolution de surface Université de Cambridge, 2003,

[9] L. Bornstein. Structures quantiques semi-conductrices. Sous-tome C ; Propriétés optiques partie 3 Vol 34. Springer

[10] W. Hamd, Elaboration par voie sol-gel et étude microstructurale de gels et de couches minces de SnO2, thèse de doctorat, Université de limoges, 2009,

[11] E. Charef, Détermination des Caractéristiques Optiques des Couches Minces du ZnO Elaborées par Spray Ultrasonique. Centre Universitaire d'EL-Ourd, 2012.

[12]بن عمر ساره – دراسة الخواص الفيزيائية للطبقات الرقيقة لاكسيد الزنك المطعم بالحديد المتوضع بتقنية رذاذ الانحلال الحراري –فيزياء المواد – جامعة قاصدي مرباح ورقلة 2016

[13] H. Benelmadjat, Elaboration et Caractérisation de Matériaux Cristallins ou Amorphes Pures et Dopés, thèse de doctorat, université de Constantine, 2011.

[14] L. Baghriche, Elaboration et Caractérisation des Couches Minces d'Oxyde de Zinc Obtenues par Pulvérisation Réactive et Spray Ultrasonique. Mémoire de magister, Université de Constantine (2006)

[15]ح. مثال دراسة الخصائص البنيوية والضوئية والكهربائية لأكسيد القصدير المطعم بالفلور المتوضع بتقنية الأمواج فوق " (2014) الصوتية " شهادة ماستر، جامعة الوادي،

[17] - W. Hamd, Elaboration par voie sol-gel et étude microstructurale de gels et de couches minces de SnO2, thèse de doctorat, Université de limoges, 2009.

[18]شراحي محمد العيد, الدراسه الطيفية لطبقات أكسيد النحاس النتوضعة على ركائز من أكسيد الزنك بالغمس

[19]- P. ROCA," Science des materiaux et techniques du reacteur dans le depot par procede plasma rf de photopiles et d'autres dispositifs en silicium amorphe hydrogene", Thèse de Doctorat, Paris 7, (1988).

[20]- Yan-mei Jiang, Thèse de Doctorat, Pulvérisation cathodique assistée par ordinateur, Thèse de doctorat, Université de Paris-Sud (1992).

[21]I.Guesmi -Dépôt De Couches Minces De Cuivre Sur Substrats Polymére De Formes Complexes Par Puluvérisation Cathodique Magnétron Avec Ionisation De La Vapeur- Thése de Doctorat – Université Paris Sud – Xi- 2011.

[22]الدكتور عزيز عقيل - مقدمة في الفيزياء الصلب -الجزء الأول القسم الأول صفحة 161

[23] K.F.Konan- B.Hartitil -B.Aka- A.Ridah -K.Dakhsi -Y.Arba Et P.Thevenin – Propriétés structurales Et Optiques de couches minces d oxyde de Zinc (ZnO) Texturées (002) par Voie Sol-Gel via spin-coating – Afrique science – Vol06(1)- 29-37- 2010 .

[24]قلاعي ايمان -تحضير و توصيف اغشية أكسيد الزنك الرقيقة النقية و المطعمة بالحديد بتقنية الرش الانحلال الحراري و اغشية أكسيد الزنك النانوية بالطريقة الكيميائية _ فيزياء الطاقوية و الطاقات المتجددة جامعة محمد خيضر بسكرة 2021

[25]مصباحي ط_دقة ع الله *تحديد بغض الخصائص اغشية أكسيد النيكل NiO المطعم بالحديد Fe* فيزياء _جامعة الشهيد حمه لخضر الوادي 2017

[26] Douglas A.Skoog FJH . and stanley R.crouch principles of Instrumental analysis 7th edition.

[27] A,Taabouche , -Etude structurale et optique de films minces ZnO elaborés par voie physique et/ ou chimique – thése doctorat – univesité fréres montouei constantine

[28] S. Sagadevan, J. Podder , optical and electical propeeties of nanocrystalline

[29] S. benhamide, J. podder , caractérisation des couches minces d oxyde de Nickle (NiO) Elaboré par spray pyrolyse , these de doctorat , Universite Mohamed Khider -Biskra 2018 .

[30] A. Derbali, L effet de la distance du Bec et la température du substrat sur les propriétés des couche minces d oxyde de zinc (ZnO) , Thése de Magister – Universite Mohamed Khider – Biskra 2011.

[31] S.sagadevan ,J.podder ,-Optical and Electric al properties of nanocistalline SnO2 thin film synthesized by chemical bath depositionmethod – solf nanoscience letters, vol.5,p.55-46,2015.

[32]بن علية زهرة *مولاي نصيرة _مساهمة في دراسة فيزيوكيميائية لرمال منطقة (تيفرنين) اليزي* فيزياء المواد _ جامعة قاصدي مرباح ورقلة 2022

[33] اسو فاطمة الزهراء _تحضير و توصيف اغشية أكسيد الزنك النقي واكسيد القصدير النقي و اختبار نشاط التحفيز الضوئي _فيزياء جامعة قاصدي مرباح ورقلة

[34] مومني جوهرة _ايدوغي عبلة _ ترسيب طبقات رقيقة على ماسند خزفية: تأثير إضافة ZrO2 في المساند _فيزياء المواد _جامعة العربي بن مهيدي ام لبواقي 2018

[35] O. Darafad, Elaboration et caractérisation des Couches Minces de sulfure de Zinc préparées par spray Ultrasonique , these de magister , université de Constantine,2010

[36]A. Rahal, Elaboration des verres conducteurs par déposition de ZnO sur des verres ordinaires. Université d ´El oued 2013

[37]عوامر وئام _اختبار أداء التحفيز الضوئي للاغشية الرقيقة متعددة الطبقات من ZnO و SnO2 المرسبة بتقنية الرش الحراري _فيزياء المواد _جامعة قاصدي مرباح ورقلة 2023

chapter3:Preparation of Thin Films and Study of their Properties

III Introduction :

This chapter outlines the methodology used to prepare samples, followed by a presentation of the results obtained from various analyses. The results are then discussed in the context of previous theoretical studies and research findings. The chapter concludes with a summary of the main findings and implications for future research.

III-1 Experimental Study :

We conducted the experiment at the Radiation and Plasma, Surfaces Physics Laboratory (LRPPS) at Kasdi Merbah University Ouargla

III-1-1 Substrate:

In our experimental work, we selected glass microscope slides as the substrate material due to their abundance and cost-effectiveness. The slides have a thickness of 1 mm, as illustrated in the following figure.

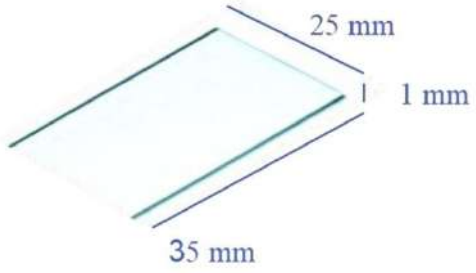

Figure (III.1): Used Glass Substrate

III 1-1-1Substrate Preparation and Cleaning:

Effective cleaning of the substrates is crucial to remove dust and impurities. The cleaning process was carried out as follows:

1. The substrate was cleaned in an ultrasonic bath containing distilled water and ethanol at room temperature for 15 minutes

. 2. The substrate was then rinsed with distilled water.

3. Finally, the substrate was dried using lint-free paper.

Figure (III.2): Ethanol bath for cleaning the substrates

III-1 1-2Preparation of Solutions:

III-1.1-3 Preparation of Solution:

First, it was necessary to clean the substrates before they were coated, with ethanol and deionized water in an ultrasonic bath for 15 min to remove any contaminants on the surface of slide substrates.

We made layer by a spin-coating sol-gel technique using a 0.2M aqueous solution of zinc acetate dihydrate (Zn (CH3COO)2. 2H2O). copper acetate was added as an copper source, with

a concentration chosen 10,20and30% to the previous solution. The precursor solution was prepared by dissolving the required amount of zinc acetate in absolute ethanol (C_2H_6O) used as the solvent whereas monoethanolamine (MEA: C2H7NO) was used as the stabilizer. The molar ratio of the precursor and the stabilizer (MEA) was kept at 1:1.The solutions were stirred for 2 h using a magnetic stirrer at 75°C to get a clear and homogeneous transparent sol, this sol was aged for 24 h. The sol was then dropped on the substrate and then it was coated for 30 s using a spin coater with 1500 rpm at ambient temperature. and then each coating was followed by subsequent drying at first at 150 °C for 10 min to evaporate the residue solvents in the film, the same procedure (spin-dry) was repeated 5 times to obtain the film with the desired thickness. At last, the final coated films were annealed in the tubular furnace for at 450°C for 90 min then let cool to room temperature.

$$m = MCV \quad \text{(III-1)}$$

- m: mass of zinc acetate

- C: concentration of the solution

- V: volume of the solution (V = 55 ml = 0.55 L)

- M: molar mass of zinc acetate

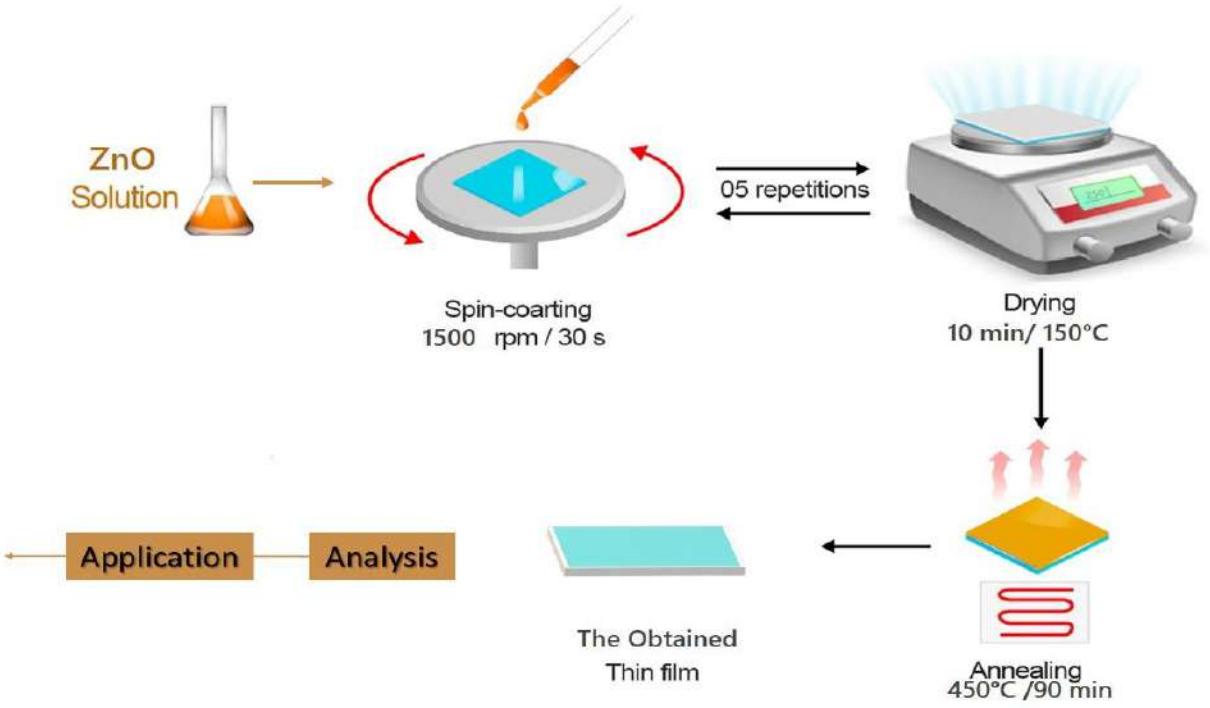

Figure II.3: Schematic of spin coating process[1].

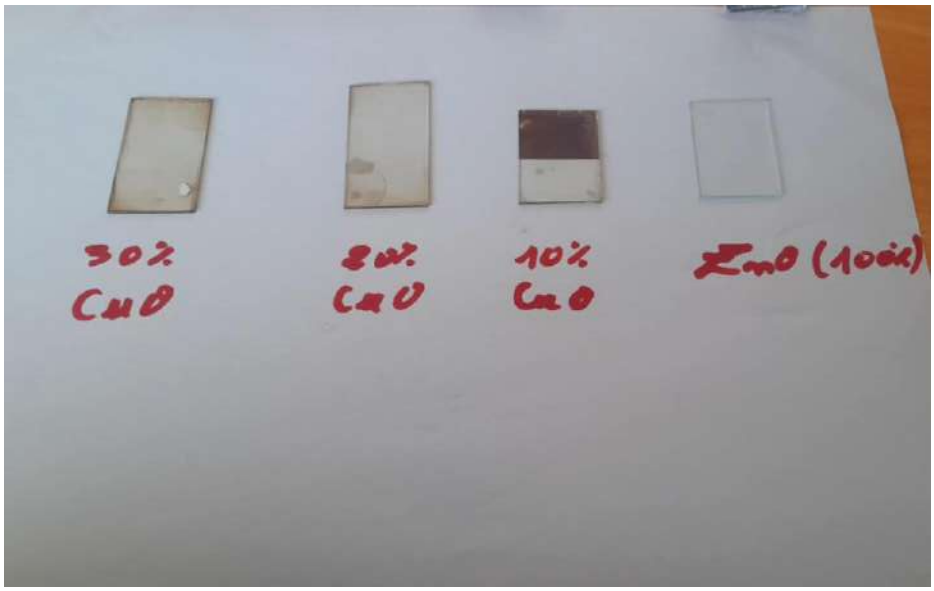

Figure III.4: The obtained films.

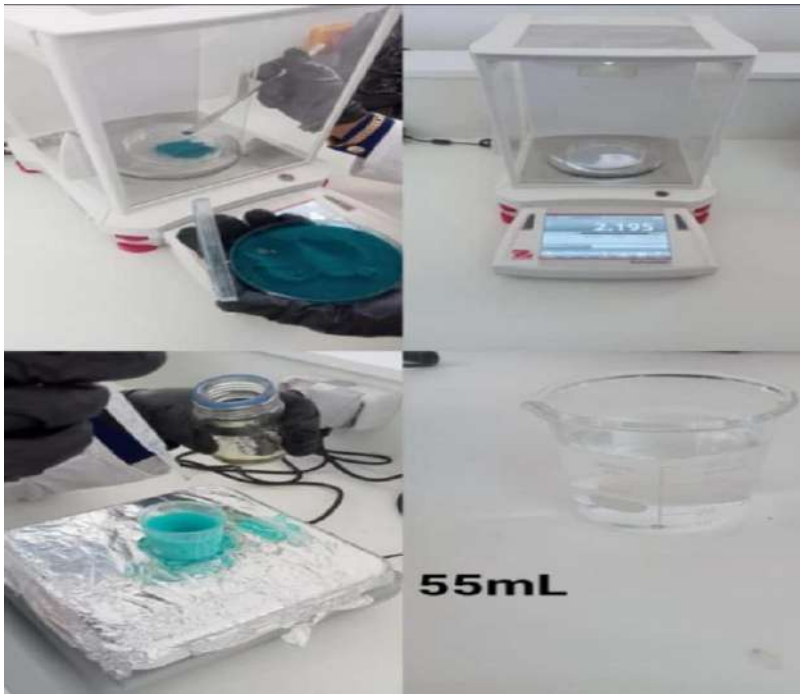

Figure (III-5): Materials and Some Equipment Used in Solution Preparation

III-2 Structural Properties:

III-2-1 X-Ray Diffraction (XRD) Analysis:

It is extremely necessary to use XRD to determine the crystalline nature and phase of the produced samples. Consequently, X-ray diffraction was used to examine the structural crystallinity in the different resultant films, scanning a 2θ (diffraction angle) between 10° and 70°, as seen in Figure III.6. As we can see from Figure III.6, the films prepared by the spray pyrolysis indicate specified reflections. at 2θ = 32.17°, 34.82°, 36.44°,57.17°,63.17°and 68.52° matching with (100), (002), (101), (002), (002) and (002) planes, respectively, according to the wurtzite hexagonal ZnO structure (JCPDS No 1-1117).

Figure III.6: The X-Ray diffraction patterns of as-sprayed films.

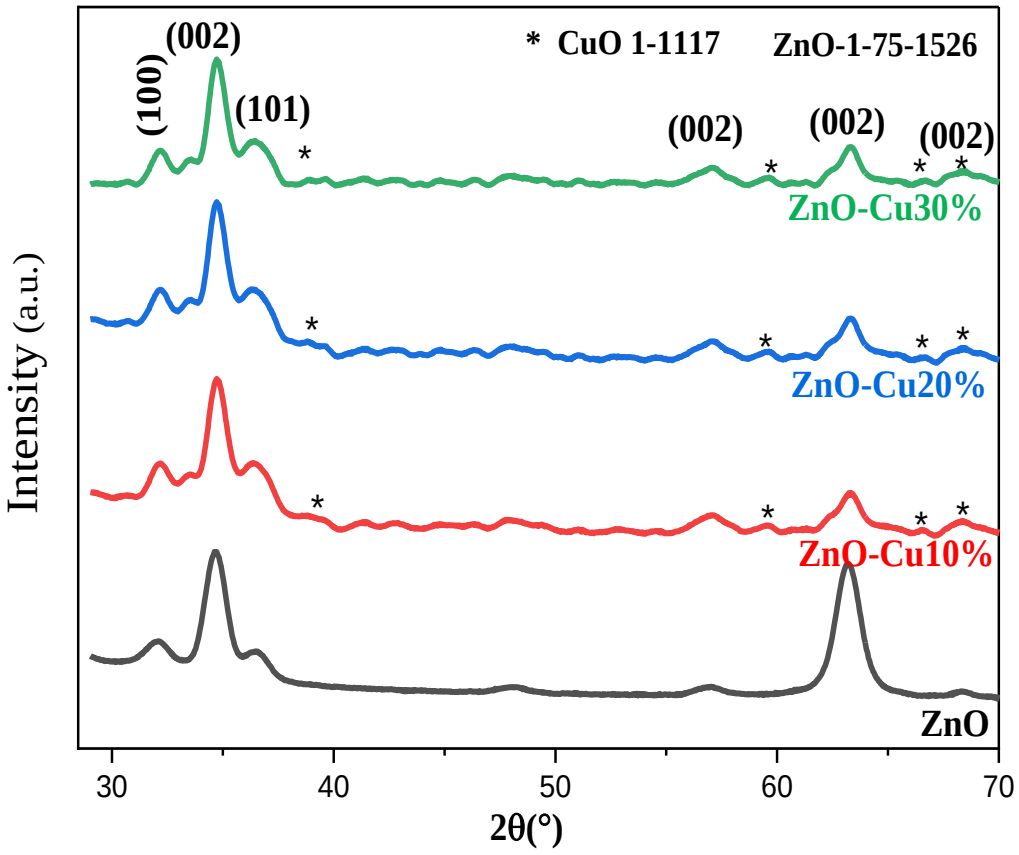

The graph plots intensity (in arbitrary units) versus 2θ (degrees), which is twice the Bragg angle. Different curves represent different compositions of ZnO-CuO films: ZnO, ZnO-Cu10%, ZnO-Cu20%, and ZnO-Cu30%. The peaks correspond to specific crystallographic planes (e.g., (100), (002), (101)). The presence and intensity of these peaks indicate the crystalline structure and phase composition of the films. The asterisk denotes peaks attributed to CuO. The graph demonstrates that increasing CuO concentration affects the intensity and position of the peaks, indicating changes in the material's crystal structure. The analysis of these patterns helps determine the success of the film deposition and the influence of CuO doping on the ZnO structure. Answer: The image displays X-ray diffraction data showing the effect of CuO doping on the crystal structure of ZnO thin films.

III-2-2 Determination of Crystallite Size:

The crystallite size (CS) was determined using the Debye-Scherrer **(II-5);** the obtained results are shown in the table below (**Table III-1**).

Table III-1: Shows the results obtained from X-ray diffraction (XRD) spectra

Samples	Phases	Cs (nm3)
CuO 0%	ZnO hexagonal	8.40
CuO10%		8.97
CuO20%		8.21
CuO30%		17.21

III-3Optical Properties:

The study of optical properties provides valuable insights into the transmittance, absorbance, and optical bandgap of the prepared samples. These properties are crucial for determining the

suitable applications of the samples. The optical behavior is closely related to the energy level structure and crystalline structure of the material.

III-3-1Transmittance Spectra:

Figure 7 illustrates the transmittance spectra of pure and ZnO-CuO-composite thin films with varying CuO concentrations (100, 10, 20, and 30%). The transmittance is plotted as a function of wavelength in the range of 300-800 nm. A slight decrease in transmittance is observed with increasing CuO concentration. However, a rapid increase in transmittance is noted in the wavelength range of 300-400 nm, reaching an average of 80% in the visible region (400 nm). This indicates that the ZnO-CuO-composite films exhibit high transparency in the visible spectrum.

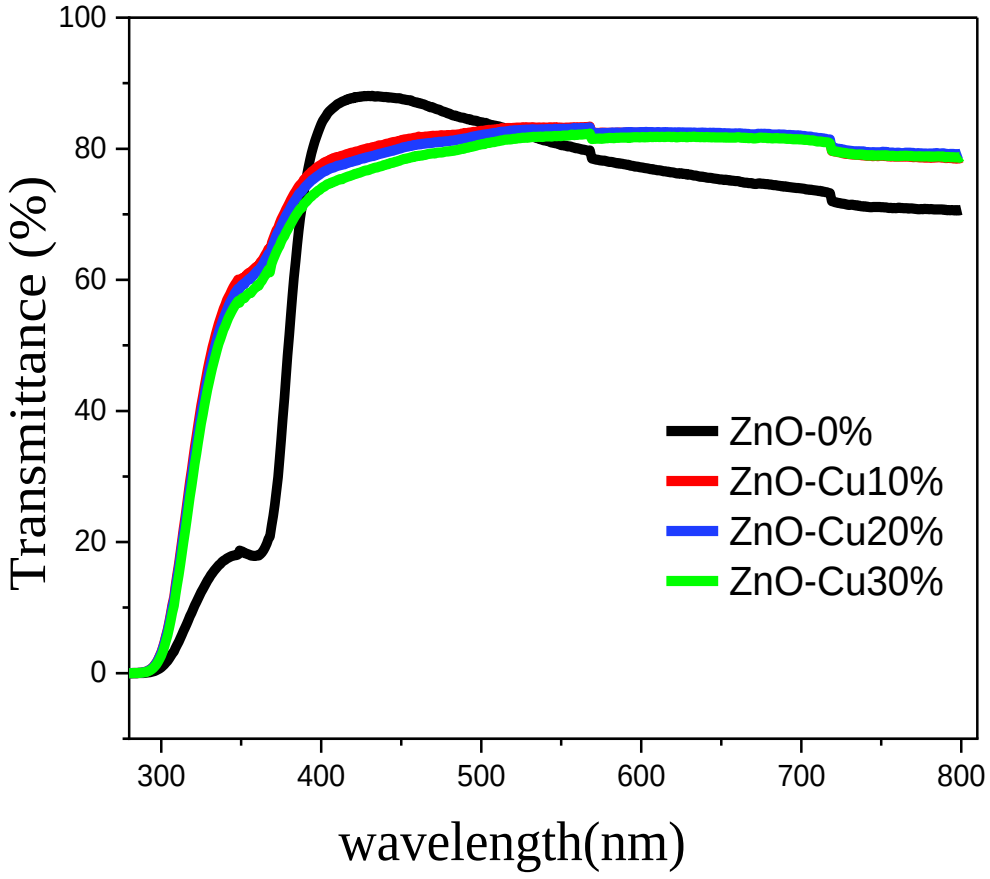

Figure III: Transmittance spectrum of as deposited thin films (ZnO, ZnO-CuO-composite)

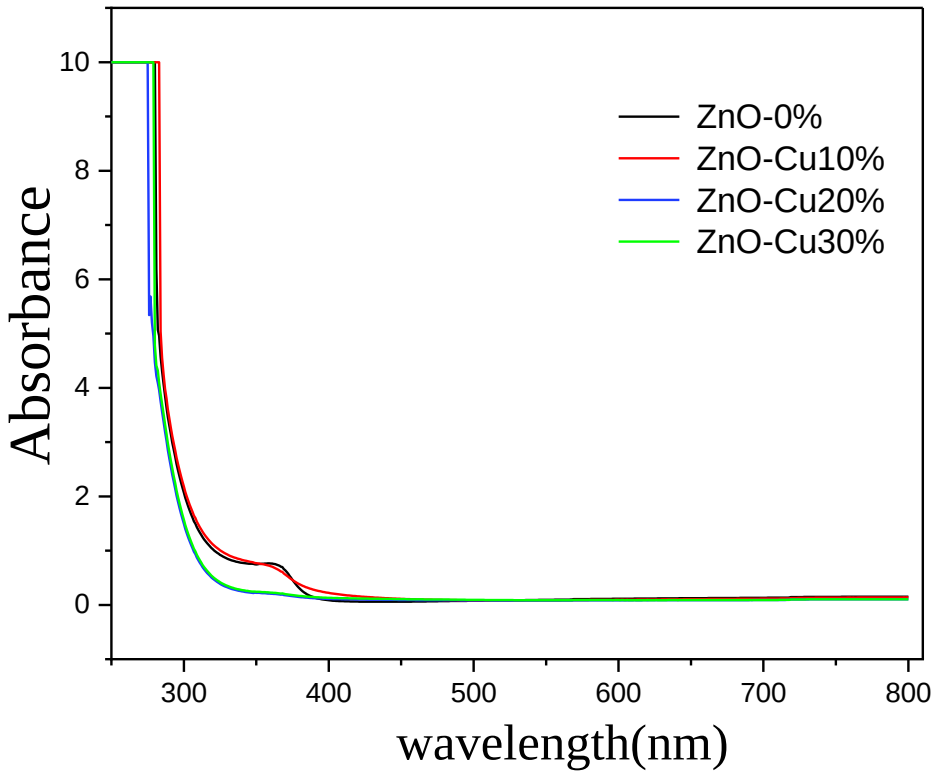

III-3- 2Absorption Spectra:

The absorption spectra of pure and ZnO-CuO-composite thin films were investigated under the same conditions as the transmittance measurements. The absorption spectra, illustrated in Figure 8, show an inverse relationship with the transmittance spectra (Figure III). The absorbance decreases with increasing wavelength and increases with increasing CuO concentration

Figure III-8: Optical Absorbance spectrum of as deposited thin films (ZnO, ZnO-CuO-composite)

III-3-3 Optical Bandgap Energy:

The optical bandgap energy is a crucial parameter in semiconductor physics, representing the minimum energy required to excite an electron from the valence band to the conduction band. The bandgap energy plays a vital role in determining the suitability of semiconducting materials for various optical applications, such as solar cells, photodetectors, and photocatalysis. The bandgap energy of ZnO and ZnO/CuO-composite thin films was determined using the Tauc relation, by plotting $(\alpha h\nu)^2$ as a function of photon energy ($h\nu$). The extrapolation of the linear part of the curve to the photon energy axis yields the optical bandgap energy for direct allowed transitions, as shown in Figure 9

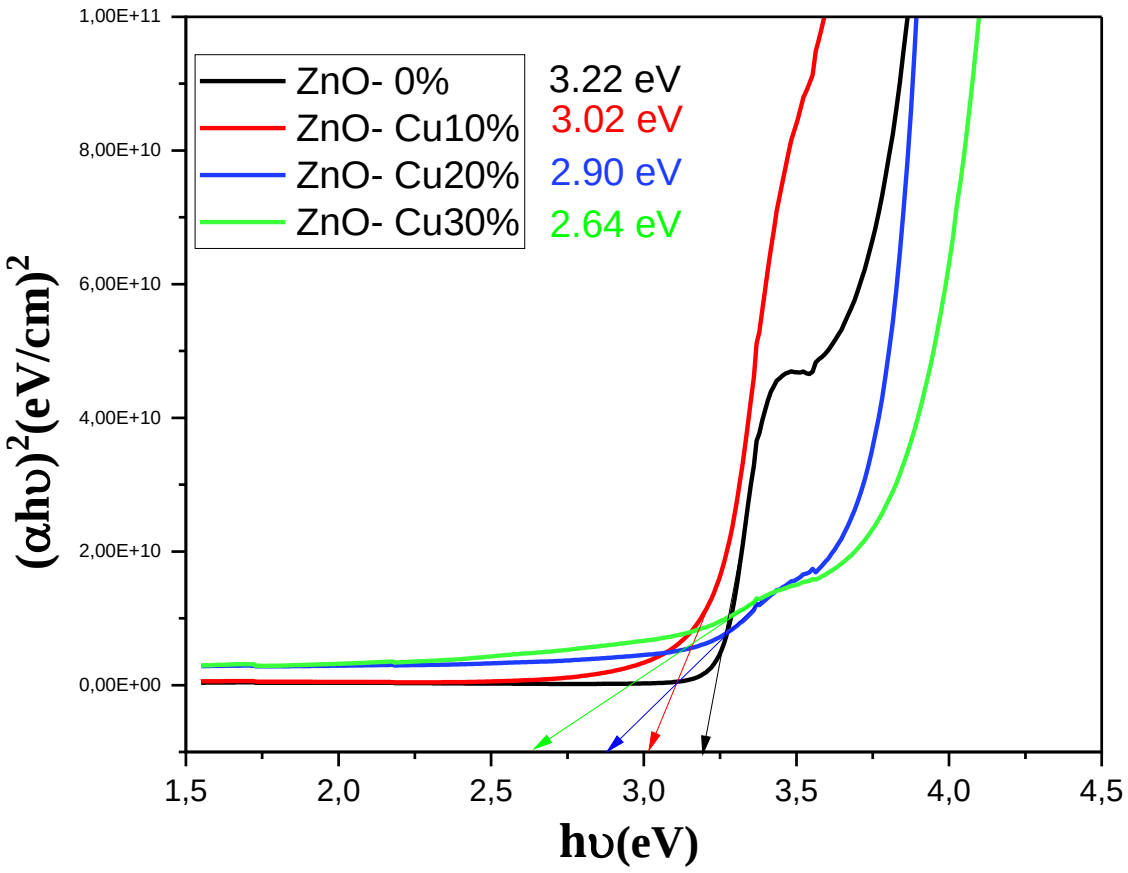

Figure III : Variation of Eg and Eu of signal and multi-layer thin films.

We find that the bandgap energies (Eg) are 3.22, 3.02, 2.91, and 2.64 eV for pure ZnO, 10%, 20%, and 30% Cu-doped samples, respectively. As we can see, the Eg values decrease with increasing CuO concentration in all cases. These results are between the intrinsic bandgap energies of ZnO and CuO (1.62 eV might not match typical values for CuO bandgap often around 1.2-1.9 eV depending on the structure, but let's assume 1.62 eV is correct for your context).

Our results indicate that the permeability decreases with increasing Cu doping concentration.

III-4 Morphological Properties:

We didn't get the expected results.

III-5 Photocatalytic Degradation:

The photocatalytic degradation of methylene blue, crystal violet, and methyl orange was investigated under sunlight irradiation. The degradation process involved the following steps:

1. Preparation of dye solutions by dissolving 5 mg of dye powder in 1 liter of distilled water.

2. Immersion of four samples of the prepared thin films in 40 ml of the dye solution, followed by stirring in the dark for 30 minutes.

3. Exposure of the samples to sunlight for 120 minutes, with 4 ml of the solution being withdrawn at regular intervals for UV-Vis spectrophotometric analysis. The results showed a gradual decrease in the intensity of the dye solution color over time, indicating degradation of the dye in the presence of the photocatalyst. The UV-Vis spectrophotometric analysis results are presented in Figure 13, which shows the absorption spectra of the dye solutions as a function of wavelength. The maximum absorption wavelengths for each dye were observed as follows:

- Methylene blue: 664 nm

- Crystal violet: 590 nm

- Methyl orange: 464 nm

The photocatalytic degradation of the dyes was investigated using pure and ZnO-CuO composite thin films as photocatalysts under sunlight irradiation.

III-5-1 MB Photocatalytic Degradation :

chapter3: Preparation of Thin Films and Study of their Properties

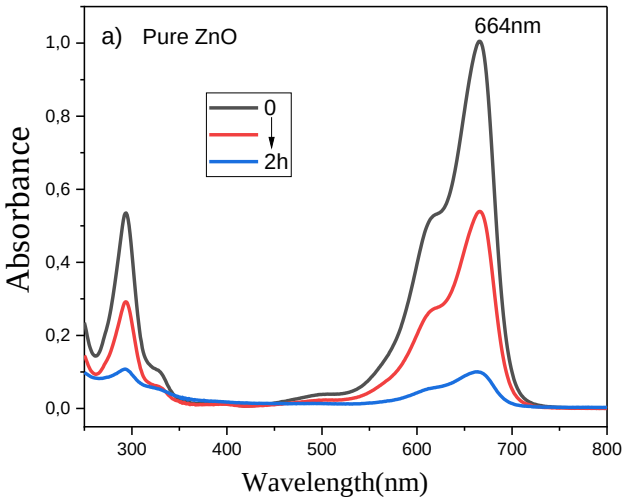
a) Pure ZnO
664nm
0
2h
Absorbance
Wavelength(nm)

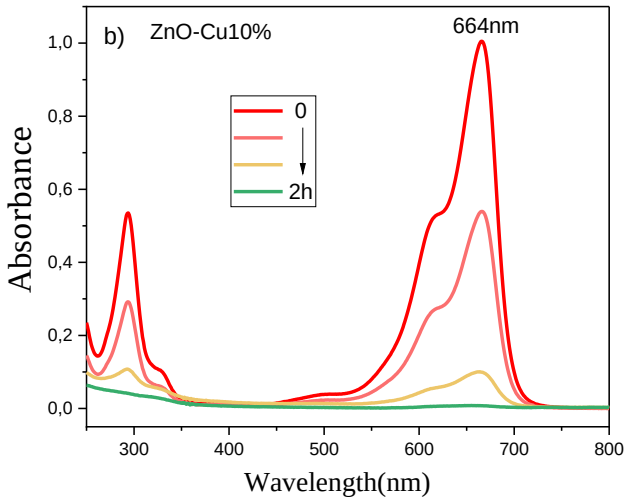
b) ZnO-Cu10%
664nm
0
2h
Absorbance
Wavelength(nm)

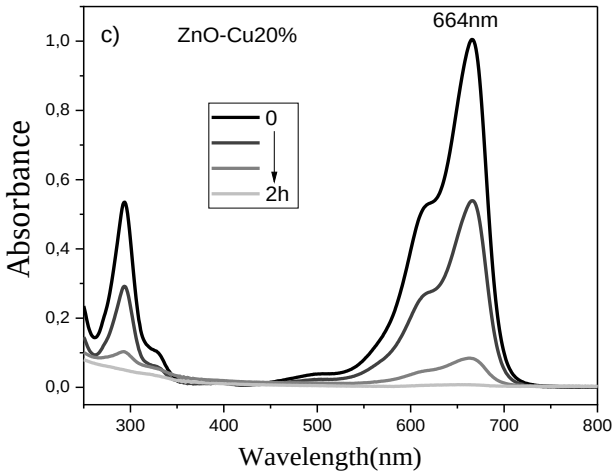
c) ZnO-Cu20%
664nm
0
2h
Absorbance
Wavelength(nm)

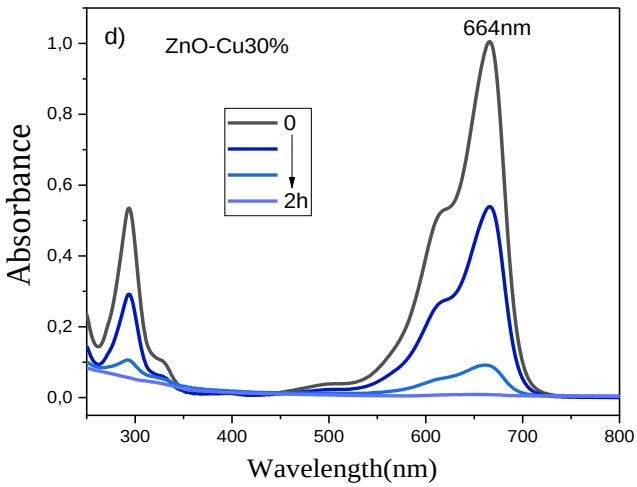
d) ZnO-Cu30%
664nm
0
2h
Absorbance
Wavelength(nm)

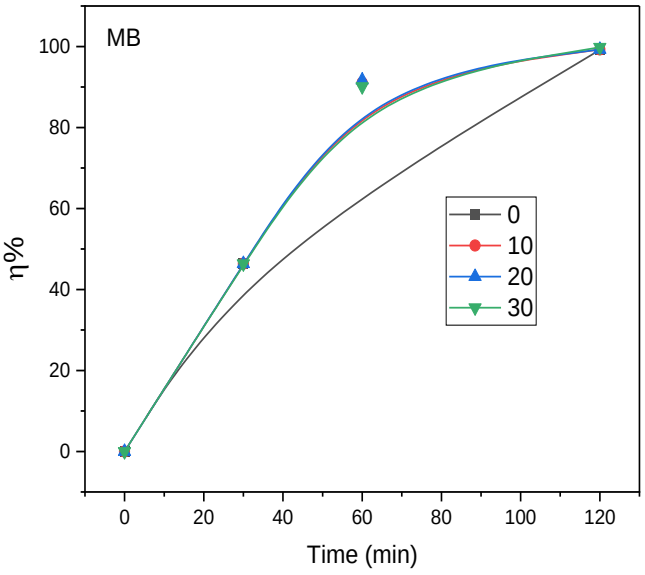
MB
0
10
20
30
η%
Time (min)

Figure III-10: UV-visible spectra of MB solution and MB photodegradation efficiency.

These graphs (a–d) depict the UV–Vis absorbance spectra of methylene blue (MB) solution after treatment with various ZnO-based photocatalysts under visible light irradiation for 0, 1, and 2 hours.

Panel (a): Pure ZnO The MB absorption peak at 664 nm decreases gradually with irradiation time, indicating degradation. After 2 hours, the absorbance is significantly reduced, but not completely eliminated, implying moderate photocatalytic activity.

Panel (b): ZnO-Cu 10% A more rapid decrease in the 664 nm peak compared to pure ZnO. * Nearly complete degradation after 2 hours, highlighting enhanced photocatalytic efficiency due to Cu doping.

Panel (c): ZnO-Cu 20% Similar trend to 10% Cu doping, with a strong decline in absorbance at 664 nm. * Slightly improved or comparable performance to ZnO-Cu10%.

Panel (d): ZnO-Cu 30% Continues the trend of efficient degradation, though possibly reaching a saturation point beyond which mor²e Cu does not significantly enhance activity.

All doped ZnO samples outperform pure ZnO. * The 664 nm peak, characteristic of MB, serves as the main indicator of photocatalytic degradation. * The Cu doping significantly accelerates the rate of MB degradation. * There may be an optimal Cu doping concentration (10–20%) beyond which additional Cu does not markedly improve performance

All samples start from 0% degradation at time zero. * Cu-doped samples show a sharp increase in degradation efficiency, especially within the first 60 minutes. * ZnO-Cu 20% and ZnO-Cu 30% reach nearly 100% degradation before 120 minutes. * Pure ZnO lags behind, reaching just under 90% at 120 minutes. * ZnO-Cu 10% also shows a marked improvement over pure ZnO, confirming the trend seen in the UV–Vis spectra.

The degradation rate and final efficiency improve with increasing Cu content, especially up to 20%. * UV–Vis spectroscopy and time-based efficiency curves confirm that the ZnO-Cu composites are more effective than pure ZnO, likely due to improved charge separation and visible light absorption facilitated by Cu ions. * The results suggest that ZnO-Cu20% may represent an optimal composition for photocatalytic applications

$$\mathbf{D}(\%) = \frac{\mathrm{Absi} - \mathrm{Absf}}{\mathrm{Absi}} \times \mathbf{100}$$

III-5-2 MO Photocatalytic Degradation:

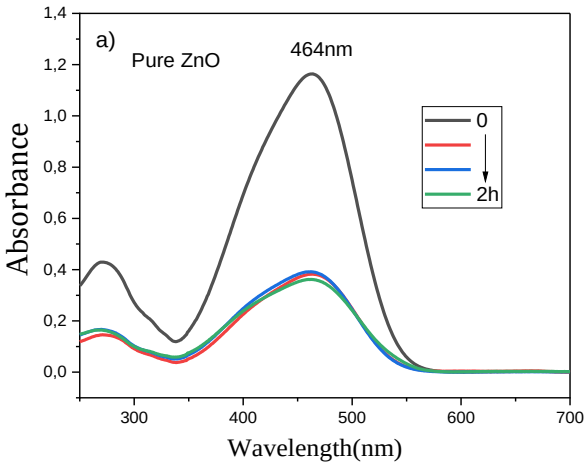
a)
Pure ZnO
464nm
0
2h
Absorbance
Wavelength(nm)

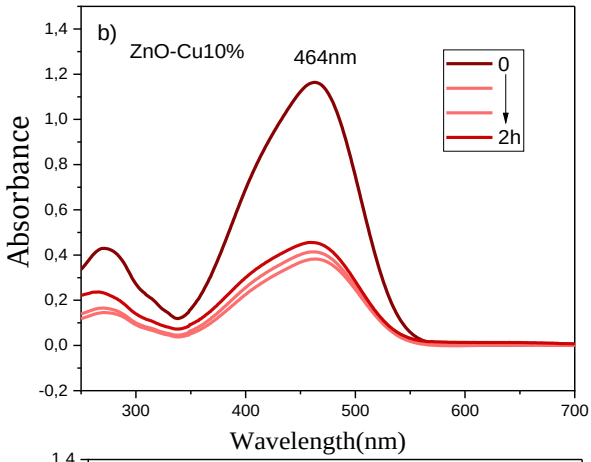
b)
ZnO-Cu10%
464nm
0
2h
Absorbance
Wavelength(nm)

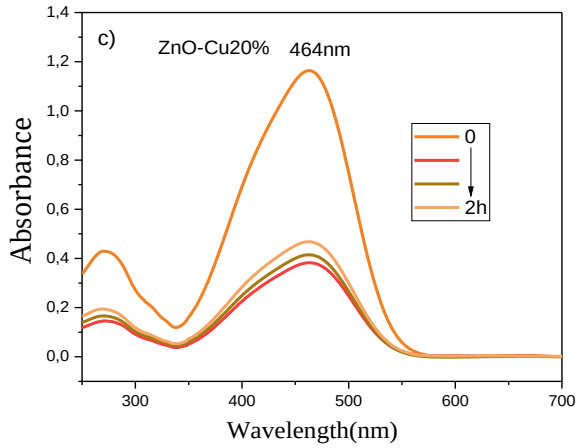
c)
ZnO-Cu20%
464nm
0
2h
Absorbance
Wavelength(nm)

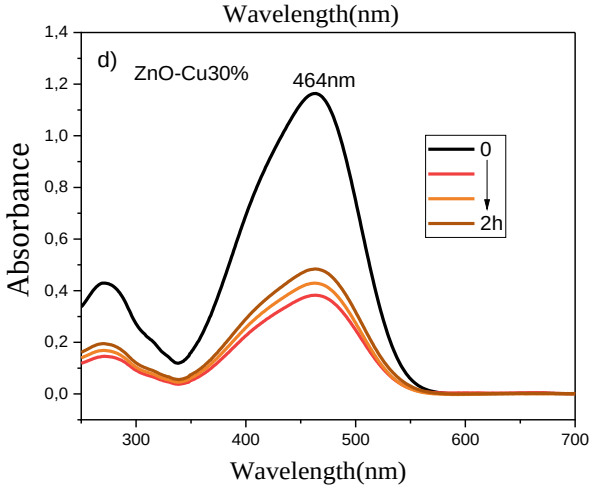
d)
ZnO-Cu30%
464nm
0
2h
Absorbance
Wavelength(nm)

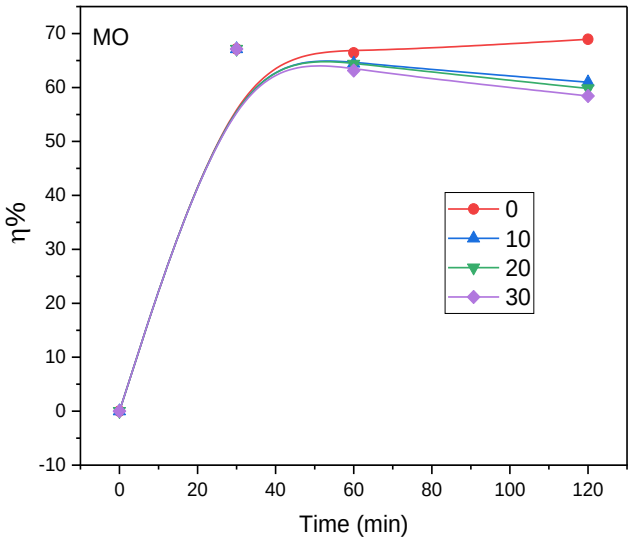
MO
0
10
20
30
η%
Time (min)

Figure III-11: UV-visible spectra of MO solution and MO photodegradation efficiency.

Top Panels (a–d): UV–Vis Absorption Spectra* These plots show the time-dependent UV–Vis absorption spectra of methyl orange (MO) in the presence of different ZnO-based photocatalysts over a period of 2 hours.

Panel (a): Pure ZnO:

- Initial absorbance at 464 nm is high, with a gradual reduction over 2 hours

.- The reduction is modest, suggesting relatively low photocatalytic activity toward MO degradation.

Panel (b): ZnO-Cu10% :

-The characteristic absorption peak of MO at 464 nm decreases with time, but the change is less pronounced than expected.

- Indicates that 10% Cu doping provides some improvement over pure ZnO but is not highly effective for MO degradation.

Panel (c): ZnO-Cu20%:

-Similar spectral pattern as ZnO-Cu10%, with limited reduction in absorbance at 464 nm

-Slight improvement is observed but remains suboptimal.

Panel (d): ZnO-Cu30%:

-Shows the highest initial absorbance and a noticeable reduction over 2 hours.

- While the decrease is more evident than in the 10% and 20% doped samples, the degradation is still incomplete, suggesting moderate activity.

All samples show limited photocatalytic degradation of methyl orange within 2 hours.

- The presence of copper (Cu) does not lead to a significant enhancement in photocatalytic performance for MO, in contrast to the case observed for methylene blue (MB) in the previous figure.

- The maximum degradation appears around 464 nm, the main absorption peak of MO.

All samples exhibit rapid degradation in the first 60 minutes, after which the efficiency plateaus. The degradation efficiency for all doping concentrations converges to around 60–70% at 120 minutes.

The trend implies that increasing Cu content beyond a certain threshold does not significantly enhance MO degradation.

Unlike MB, where Cu doping greatly improved performance, MO degradation seems to be less responsive to Cu modification of ZnO.

The characteristic MO absorption peak at 464 nm decreases over time for all samples, but not substantially.

Doping ZnO with Cu at 10%, 20%, and 30% slightly improves the photocatalytic activity, but the enhancement is not significant.

This suggests that methyl orange is more resistant to photocatalytic degradation with these materials, or that Cu doping does not promote favorable interactions with MO molecules.

Further optimization, possibly with different dopants or synthesis conditions, may be required to achieve higher degradation efficiencies for MO

III-5-3 CV Photocatalytic Degradation:

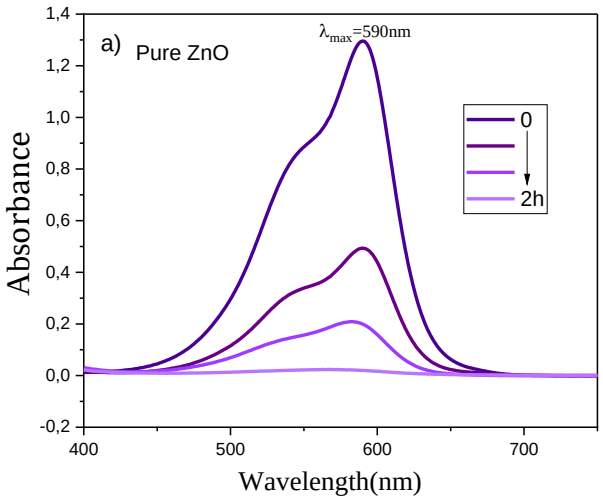
a) Pure ZnO
λmax=590nm
Absorbance
Wavelength(nm)
0
2h

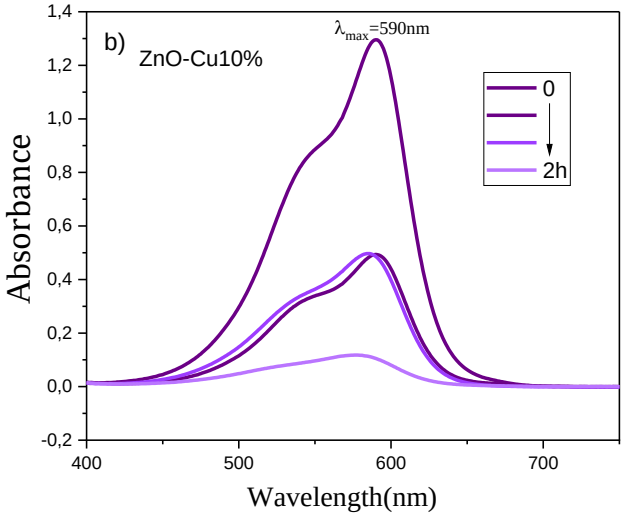
b) ZnO-Cu10%
λmax=590nm
Absorbance
Wavelength(nm)
0
2h

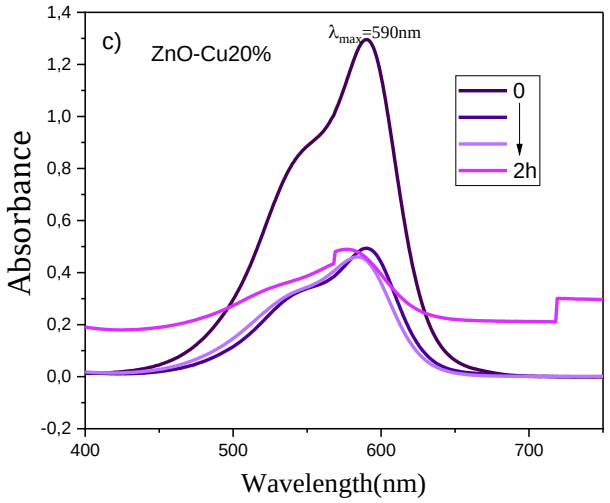
c) ZnO-Cu20%
λmax=590nm
Absorbance
Wavelength(nm)
0
2h

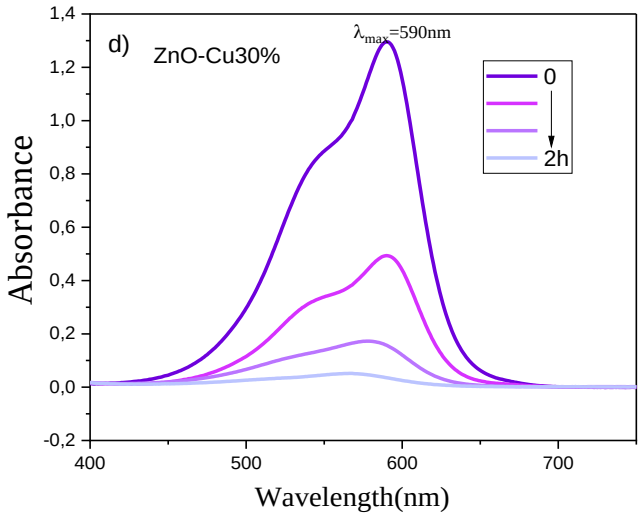
d) ZnO-Cu30%
λmax=590nm
Absorbance
Wavelength(nm)
0
2h

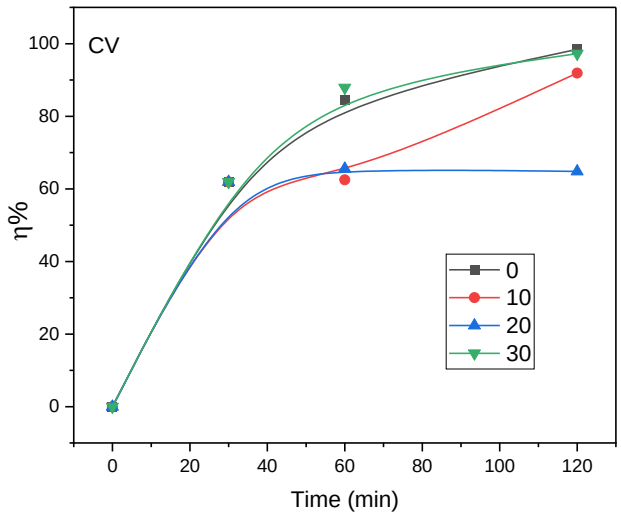
CV
η%
Time (min)
0
10
20
30

Figure III-12: UV-visible spectra of CV solution and CV photodegradation efficiency

crystal violet (CV) dye using pure ZnO and Cu-doped ZnO nanomaterials under visible light irradiation:

Top Panels (a–d): UV–Vis Absorption SpectraThese plots show the absorption spectra of crystal violet (CV) in the presence of various ZnO-based photocatalysts over a 2-hour irradiation period. The key absorption peak of CV appears at λ_{max} = 590 nm, serving as an indicator of dye degradation.

-Panel (a): Pure ZnO Shows a gradual decrease in the 590 nm absorbance peak after 2 hours of irradiation. Indicates moderate photocatalytic activity of undoped ZnO for CV degradation.

-Panel (b): ZnO-Cu 10% More rapid decline in the absorption intensity at 590 nm compared to pure ZnO. This suggests that Cu doping at 10% enhances photocatalytic performance by improving charge separation and visible light absorption.

-Panel (c): ZnO-Cu 20% The degradation trend slows down compared to 10% doping, and unusual noise appears in the spectrum at longer wavelengths (>650 nm), possibly due to experimental artifact or scattering. This may indicate a less efficient or less stable photocatalytic system at this doping level.

-Panel (d): ZnO-Cu 30% Shows a relatively consistent and smooth decrease in absorbance at 590 nm, indicating sustained photocatalytic activity. However, its performance appears slightly lower than ZnO-Cu10%, suggesting that excessive Cu doping may hinder optimal activity, potentially due to recombination centers or structural changes.

All samples show a downward trend in absorbance at 590 nm, confirming photocatalytic degradation. ZnO-Cu10% exhibits the best balance of degradation rate and stability for CV dye.
* Overdoping with Cu (20% or 30%) does not lead to further improvements and might even reduce activity.

Analysis:

ZnO-Cu10% achieves the highest efficiency (\~100%) after 120 minutes, showing superior photocatalytic performance.

-Pure ZnO reaches approximately 80–85% degradation efficiency at 120 min.

ZnO-Cu20% shows reduced performance (\~60%), possibly due to over-doping effects.

ZnO-Cu30% shows better performance than 20% but still below 10%, indicating a non-linear relationship between Cu content and efficiency

Optimal performance is observed for ZnO-Cu10%, achieving near-complete degradation within 2 hours. Higher Cu content (20–30%) leads to diminished or plateaued performance, likely due to the formation of recombination centers or decreased crystallinity. The UV–Vis spectra and kinetic degradation data complement each other, affirming that moderate Cu doping enhances photocatalytic activity, while excessive doping may be counterproductive.

III-5-4 pH Effect on the photocatalytic degradation rate:

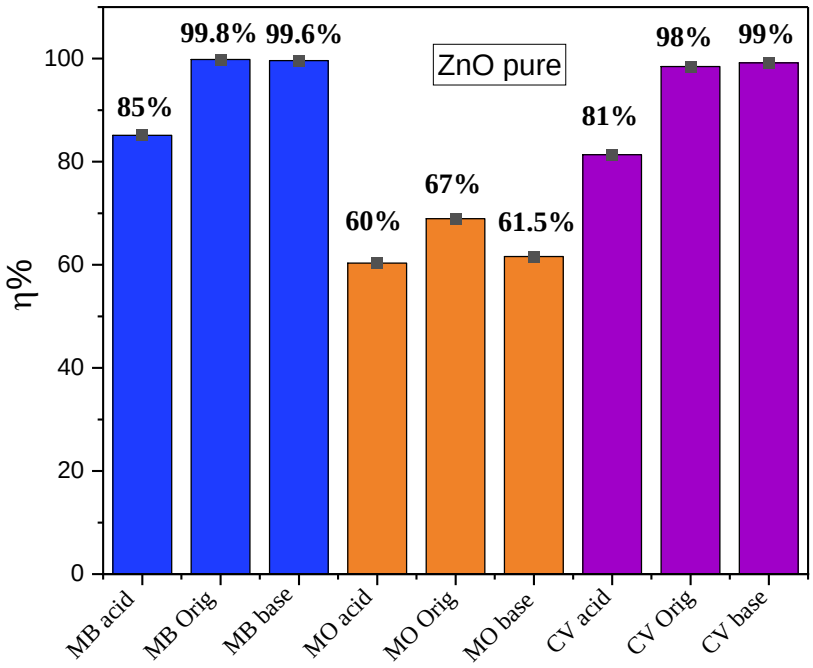

Figure.III 13: The photodegradation efficiencies of various pH levels(ZnO pure) .

The bar chart illustrates the photocatalytic degradation efficiency (η%) of pure ZnO for three different dyes Methylene Blue (MB), Methyl Orange (MO), and Crystal Violet (CV) under three different pH conditions: acidic, original (neutral), and basic.

1. **Methylene Blue (MB): Acidic:** 85% **Original:** 99.8% **Basic:** 99.6%

➢ ZnO shows very high photocatalytic activity in neutral and basic conditions for MB, suggesting MB is efficiently degraded by ZnO in both environments.

2.Methyl Orange (MO):Acidic: 60% Original: 67% Basic: 61.5%

➢ The efficiency is relatively low for MO across all pH conditions, with the highest degradation in neutral medium. This may suggest lower interaction or adsorption of MO on ZnO surface or less favorable degradation kinetics.

3.Crystal Violet (CV): Acidic: 81% Original: 98% Basic: 99%

➢ ZnO shows excellent efficiency for CV in neutral and basic media, similar to MB, but with a noticeable drop under acidic conditions.

ZnO exhibits higher photocatalytic efficiency in neutral and basic media, particularly for MB and CV, The MO dye shows significantly lower degradation*, indicating it is less reactive or less adsorbed onto ZnO under the given conditions.

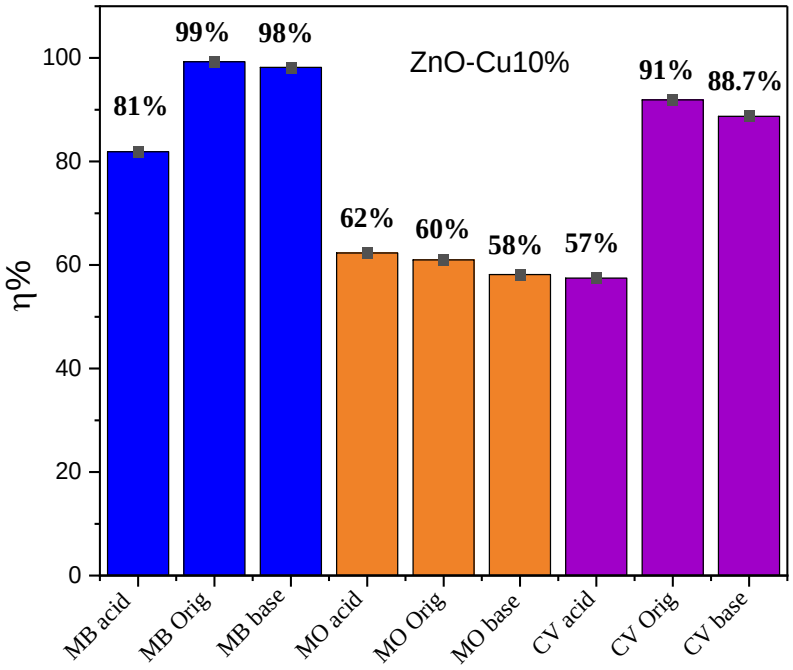

Figure III.14: The photodegradation efficiencies of various pH levels. (ZnO-Cu10%)

– ZnO-Cu 10% This bar chart presents the photocatalytic degradation efficiency (η%) of ZnO doped with 10% Cu (ZnO-Cu 10%) for three dyes under different pH conditions (acidic, original, and basic):

1. Methylene Blue (MB): Acidic: 81% Original: 99% Basic: 98% Interpretation: High efficiency in both original and basic media (similar to pure ZnO). Slight decrease under acidic conditions. Copper doping had no significant effect here as ZnO was already highly efficient in MB degradation.

2. Methyl Orange (MO): Acidic: 62% Original: 60% Basic: 58% Interpretation: Low photocatalytic efficiency across all media, similar or slightly worse than with pure ZnO (which ranged from 60–67%). Copper doping did not improve degradation of MO, possibly due to poor adsorption or weak interaction between MO and the catalyst surface.

3. Crystal Violet (CV): Acidic: 57% Original: 91% Basic: 88.7% Interpretation: Efficiency significantly dropped in acidic medium (from 81% with pure ZnO to 57%). Efficiency in original and basic conditions remained high but was lower than pure ZnO (which reached 98–99%). Comparison Table: Pure ZnO vs ZnO-Cu 10% DyeZnO Pure (Original)ZnO-Cu 10% (Original)Effect of Cu DopingMB99.8%99%No significant changeMO67%60%Slightly worseCV98%91%Noticeable decrease Scientific Insight: Cu^{2+} ions may act as electron traps, preventing electron-hole recombination and enhancing activity, but: In some cases (e.g., CV in acid), copper may introduce surface states that hinder activity.

Doping can also affect light absorption properties and dye–surface interactions differently depending on the dye structure. MB degradation remained excellent. MO degradation was still ²poor — doping had minimal effect. CV degradation efficiency declined, especially in acidic medium.

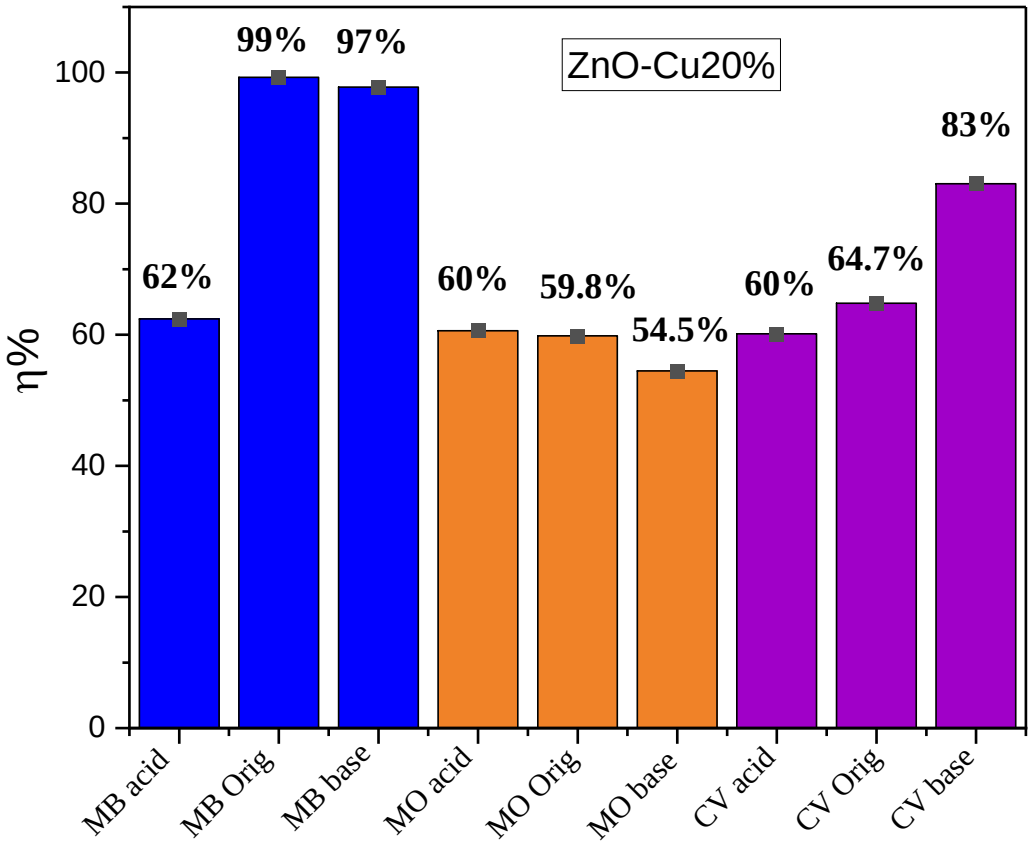

Figure III.15: The photodegradation efficiencies of various pH levels. (ZnO-Cu20%) The bar chart shows the percentage of ZnO-Cu20% for different treatments (acid, original, base) and materials (MB, MO, CV):

MB (Material B): Acid treatment: 62% Original: 99% Base treatment: 97% MO (Material O): Acid treatment: 60% Original: 59.8% Base treatment: 54.5% CV (Material V): Acid treatment: 60% *Original: 64.7% Base treatment: 83% The chart illustrates how different treatments and materials affect the percentage of ZnO-Cu20%. The highest percentage (99%) is observed for material B in its original state. Material V shows a significant increase in ZnO-Cu20% after base treatment (83%). The lowest percentage (54.5%) is found in material O after base treatment. Answer: The provided chart displays the percentage of ZnO-Cu20% under various conditions.

The highest percentage is 99% (MB original), and the lowest is 54.5% (MO base).

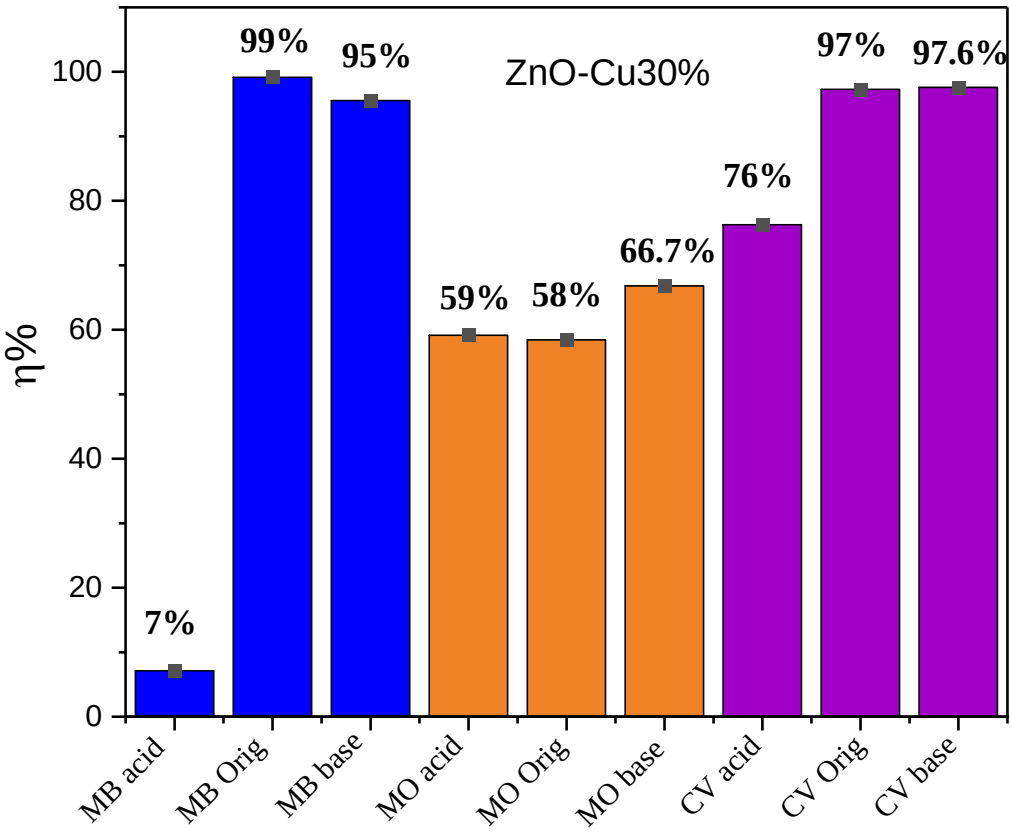

Figure III.16: The photodegradation efficiencies of various pH levels(ZnO-Cu30%)

the bar chart showing the percentage of ZnO-Cu30% under different conditions (MB acid, MB Orig, MB base, MO acid, MO Orig, MO base, CV acid, CV Orig, CV base).

The chart shows the following percentages: MB acid: 7% MB Orig: 99% MB base: 95% MO acid: 59% MO Orig: 58% MO base: 66.7% CV acid: 76% CV Orig: 97% CV base: 97.6% The chart illustrates how the percentage of ZnO-Cu30% varies depending on the treatment applied (acid, original, base) and the type of treatment (MB, MO, CV). The highest percentages are observed in the original and base treatments for MB and CV, while the lowest percentage is found in the MB acid treatment. The MO treatments show intermediate percentages. Answer: The bar chart displays the percentage of ZnO-Cu30% under various conditions.

with the highest percentage (97.6%) observed in the CV base treatment and the lowest (7%) in the MB acid treatment.

References

[1] B.SAFA -synthesis and characterization of thin films based on functional metal oxides – LMD doctorate – UNIVERSITY OF KASDI MERBAH OUARGLA 2024.

بالهاني سمية-تحضير و معاينة الطبقات الرقيقة من اكسيد الزنك المطعم بالمغنيزيوم و اختبار اداءها في التحفيز .
الضوئي[2]

Conclusion

Conclusion

The research presented in this work provides a comprehensive investigation into the synthesis, characterization, and functional evaluation of transparent conducting oxide (TCO) thin films based on zinc oxide (ZnO) and copper-doped ZnO (ZnO:Cu). The study is grounded in the increasing demand for multifunctional materials that exhibit both high optical transparency and semiconducting behavior for use in advanced technologies such as solar cells, sensors, smart windows, and photocatalytic systems.

The preparation of the thin films was conducted using the sol-gel spin-coating technique—a low-cost, scalable, and efficient method for producing high-quality oxide films. In this approach, zinc acetate dihydrate served as the Zn precursor, while copper acetate was introduced at varying concentrations (10%, 20%, and 30%) to investigate the influence of Cu doping on the structural and functional properties of ZnO. Monoethanolamine (MEA) was used as a stabilizing agent, and ethanol acted as the solvent. The precursor solutions were magnetically stirred at elevated temperature to ensure homogeneity and subsequently aged to form a stable and clear sol. The spin-coating process was employed to deposit the films on glass substrates, followed by sequential drying and annealing steps to achieve well-adhered and crystallized oxide layers.

The structural analysis, primarily using X-ray diffraction (XRD), confirmed the formation of a hexagonal wurtzite structure in pure and Cu-doped ZnO films. The incorporation of Cu ions resulted in subtle shifts in peak positions and intensities, suggesting successful doping and minor lattice distortions. Crystallite size analysis showed that doping influenced the grain size, which in turn could affect electronic and optical behavior. These structural insights are crucial, as they reveal how doping can tailor the microstructure and, hence, the macroscopic properties of the films.

Optical measurements, including transmittance and absorbance spectra, demonstrated that all samples maintained high transparency in the visible spectrum, with pure ZnO reaching up to 80% transmittance. However, increased Cu doping led to a reduction in transparency, which is consistent with the introduction of mid-gap states and increased scattering centers. The optical bandgap, determined using the Tauc method, exhibited a narrowing trend with higher Cu concentrations, decreasing from approximately 3.22 eV in pure ZnO to 2.64 eV in ZnO-Cu30%. This bandgap modulation is significant for applications requiring specific absorption thresholds, such as visible-light photocatalysis or UV filtering.

Photocatalytic performance was evaluated through the degradation of organic dyes—methylene blue, methyl orange, and crystal violet—under natural sunlight. The results indicated that ZnO-Cu10% exhibited the highest degradation efficiency, surpassing even the pure ZnO samples. This improvement is attributed to the reduced recombination of photogenerated electron-hole pairs facilitated by Cu incorporation, which enhances charge carrier mobility and prolongs their lifetime. However, further increases in Cu content (20% and 30%) led to decreased efficiency, likely due to the formation of recombination centers and phase segregation, which hindered catalytic performance.

The degradation efficiencies were also studied under different pH conditions, revealing that both acidic and basic environments influenced the photocatalytic behavior. These findings

support the idea that both the material properties and environmental conditions play pivotal roles in determining photocatalytic outcomes.

In conclusion, the sol-gel spin-coating method proved to be a reliable and versatile technique for fabricating high-quality ZnO-based thin films. The incorporation of copper into ZnO matrices allowed fine-tuning of structural, optical, and photocatalytic properties. Moderate doping levels—especially 10% Cu—yielded the best balance between transparency and catalytic activity, making these films promising candidates for environmental remediation applications and optoelectronic devices. Future studies may explore the use of other dopants, multilayer architectures, or hybrid organic-inorganic composites to further enhance performance and broaden the scope of applications.

ملخص

تم في هذا البحث تصنيع أغشية رقيقة من أوكسيد الزنك (ZnO) مطعّمة بعنصر النحاس بنسب مختلفة (10%، 20%، و30%)، باستخدام تقنية السول-جيل المقترنة بالطلاء الدوراني .(spin coating) استُخدمت خلات الزنك الثنائية بتركيز 0.2 مول/لتر كمصدر للزنك، وخلات النحاس كمصدر للتطعيم، وتمت عملية الترسيب على شرائح زجاجية نظيفة في درجة حرارة الغرفة داخل مخبر الإشعاع والبلازما وفيزياء السطوح.(LRPPS)

بعد التحضير، خضعت العينات لتحليل شامل لتحديد خواصها البنيوية والبصرية والمورفولوجية. أظهرت نتائج حيود الأشعة السينية (XRD) وجود بنية متعددة التبلور لأوكسيد الزنك، محافظة على الشكل السداسي المعروف (wurtzite) حتى بعد إدخال النحاس.

من الناحية البصرية، أظهرت الأغشية شفافية عالية في المجال المرئي، حيث بلغت نسبة النفاذية نحو 95%، مع انخفاض طفيف مع زيادة نسبة النحاس. كما أُجريت حسابات لفجوة الطاقة باستخدام طريقةTauc ، والتي أظهرت انخفاضًا تدريجيًا في قيمة فجوة الطاقة من 2.46 eV إلى 3.22 eV مع زيادة تركيز عنصر التطعيم، مما يشير إلى تأثير مباشر للنحاس على البنية الإلكترونية للمادة.

لم نتحصل على نتائج المجهر الإلكتروني الماسح. (SEM)

تم اختبار الفعالية التحفيزية الضوئية لهذه الأغشية من خلال تعريضها لضوء الشمس الطبيعي في مدينة ورقلة، واستخدامها في إزالة ثلاثة أصباغ عضوية ملوثة: أزرق المثيلين(MB) ، الكريستال البنفسجي (CV)، وبرتقالي المثيل .(MO) أظهرت النتائج أن الأغشية، خاصة عند تركيز 10% من النحاس، تمتلك قدرة فعالة على تفكيك الملوثات العضوية، حيث وصلت كفاءة التحلل الضوئي لأزرق المثيلين إلى .80%.

Abstract

This study focuses on the preparation of zinc oxide (ZnO) thin films doped with different concentrations of copper (10%, 20%, and 30%) using the sol-gel method combined with the spin coating technique. The precursor solution consisted of 0.2 M zinc acetate as the zinc source and copper acetate as the doping agent. The films were deposited on pre-cleaned glass substrates at room temperature in the Laboratory of Radiation, Plasma, and Surface Physics (LRPPS).

The samples were subjected to structural and optical characterization. X-ray diffraction (XRD) results confirmed that the films retained the hexagonal wurtzite structure of ZnO and exhibited a polycrystalline nature, even after copper incorporation.

Optically, the films showed high transparency in the visible range, reaching approximately 95%, with a slight decrease as copper concentration increased. The optical bandgap was calculated using the Tauc model, revealing a reduction in energy gap values from 3.22 eV to 2.46 eV, indicating that Cu doping alters the electronic structure of the films.

Scanning Electron Microscopy (SEM) analysis was not available.

The photocatalytic activity of the films was evaluated under natural sunlight in Ouargla, using the films to degrade three organic dyes: Methylene Blue (MB), Crystal Violet (CV), and Methyl Orange (MO). Results showed that the film doped with 10% Cu achieved the highest degradation efficiency for MB, reaching up to 80%, confirming the promising potential of these materials in environmental applications.

Résumé

Cette étude porte sur la préparation de couches minces d'oxyde de zinc (ZnO) dopées au cuivre à différentes concentrations (10 %, 20 % et 30 %) à l'aide de la méthode sol-gel combinée à la technique de spin coating. La solution précurseur contenait de l'acétate de zinc (0,2 M) comme source de Zn et de l'acétate de cuivre comme agent dopant. Les couches ont été déposées sur des lames de verre propres à température ambiante dans le laboratoire de rayonnement, plasma et physique des surfaces (LRPPS).

Les échantillons ont été caractérisés sur les plans structurel et optique. Les analyses par diffraction des rayons X (XRD) ont montré que les films conservent la structure hexagonale wurtzite du ZnO, tout en présentant un caractère polycristallin, même après le dopage au cuivre.

Sur le plan optique, les couches ont montré une transparence élevée dans la région visible (~95 %), avec une légère diminution à mesure que la concentration en cuivre augmente. La bande interdite optique a été déterminée selon le modèle de Tauc, montrant une réduction des valeurs de 3,22 eV à 2,46 eV, ce qui indique une modification de la structure électronique des couches due au dopage.

L'analyse par microscope électronique à balayage (MEB) n'a pas été réalisée.

L'activité photocatalytique des films a été évaluée sous lumière solaire naturelle à Ouargla, en testant la dégradation de trois colorants organiques : Bleu de méthylène (MB), Violet de cristal (CV) et Orange de méthyle (MO). Les résultats ont révélé que le film dopé à 10 % de cuivre présentait la meilleure efficacité, atteignant un taux de dégradation de 80 % pour le bleu de méthylène, confirmant ainsi le potentiel de ces matériaux dans les applications de dépollution.